

Reactions forming $C_{n=2,10}^{(0,+)}$, $C_{n=2,4}H^{(0,+)}$ and $C_3H_2^{(0,+)}$ in the gas phase: semi empirical branching ratios.

M. Chabot¹, K. Béroff², P. Gratier³, A. Jallat¹, V. Wakelam^{4,5}

ABSTRACT

The aim of this paper is to provide a new set of branching ratios for interstellar and planetary chemical networks based on a semi empirical model. We applied, instead of zero order theory (i.e. only the most exoergic decaying channel is considered), a statistical microcanonical model based on the construction of breakdown curves and using experimental high velocity collision branching ratios for their parametrization. We applied the model to ion-molecule, neutral-neutral, and ion-pair reactions implemented in the few popular databases for astrochemistry such as KIDA, OSU and UMIST. We studied the reactions of carbon and hydrocarbon species with electrons, He^+ , H^+ , CH^+ , CH , C , and C^+ leading to intermediate complexes of the type $C_{n=2,10}$, $C_{n=2,4}H$, C_3H_2 , $C_{n=2,10}^+$, $C_{n=2,4}H^+$, or $C_3H_2^+$. Comparison of predictions with measurements supports the validity of the model. Huge deviations with respect to database values are often obtained. Effects of the new branching ratios in time dependant chemistry for dark clouds and for photodissociation region chemistry with conditions similar to those found in the Horsehead Nebula are discussed.

Subject headings: Physical data and processes: astrochemistry — Astronomical databases: miscellaneous — ISM: abundances, molecules

1. Introduction

Carbon nuclei are produced by the triple alpha reaction (Salpeter 1952) inside stars during Helium burning. Dying stars in the asymptotic giant branch (AGB) and super nova explosions (SNe) II are the two main classes of stars that are responsible for the total amount of carbon into the galaxy today (Clayton 2003). In interstellar medium (ISM), carbon nuclei may be observed in atomic and ionic forms. They also form the backbone of a huge number of molecules observed in the gas phase, from the most stable diatomic ones such as CO (Dame et al. 2001) to the large polyatomic species such as PAH (Tielens 2008). Carbon is also contained in various condensed matter in

the form of grains such as hydrogenated amorphous carbon (HAC), carbon dusts, diamond, ... (Dartois 2011, and references therein). Carbon is present in ices (Tielens et al. 1991) and in large carbon based molecular structures mixed with silicated material grains found in primitive carbonaceous meteorites on earth (Alexander et al. 2007).

It is believed that carbon dusts are strongly produced by AGB stars and type II SNe (Matsuura et al. 2009). In their release phases, ions, atoms, simple molecules and more complex ones are also synthesized. From star ejecta three types of carbonaceous matter (i.e. atomic, molecular and dust) is injected in the surrounding ISM and will dynamically evolve. The solid reservoir may be transformed partly or totally in molecular form and/or atomic form by shocks (Jones et al. 1990; Tielens et al. 1994) or/and UV (Scott et al. 1997) and/or particle collisions (Godard et al. 2011). On the other hand, atoms and/or molecules could condensate to form solids and ices on existing grains (Allamandola et al. 1999). Chemical reactions in the gas phase will modify the chemical composition of ISM. Reaction of atoms and/or

¹Institut de Physique Nucléaire d'Orsay, IN2P3-CNRS and Université Paris-Sud, 91406 Orsay cedex, France

²Institut des Sciences Moléculaires d'Orsay, CNRS and Université Paris-Sud, 91405 Orsay cedex, France

³Institut de Radioastronomie Millimétrique, 300 rue de la Piscine, 38406 Saint Martin d'Hères, France

⁴Univ. Bordeaux, LAB, UMR 5804, F-33270, Floirac, France

⁵CNRS, LAB, UMR 5804, F-33270, Floirac, France

molecules at the surface of (icy) grains will play also an important role in the chemical evolution of the carbon (Garrod & Herbst 2006).

In all these complex and dynamically coupled processes, gas - phase chemistry is certainly the easiest subject to tackle. Indeed, since it involves two body reactions, measurements and/or calculations are possible with few assumptions. In contrast, chemistry at the surface of grains and chemistry resulting from desorption/erosion are speculative since the composition and morphology of grains are poorly known. Thanks to intense studies by molecular physicists and/or chemists, large databases with thousands of reaction rate coefficients such as KIDA (Wakelam et al. 2012), OSU (Prasad & Huntress 1980), or UDFa (Woodall et al. 2007; McElroy et al. 2013) exist for gas-phase ISM chemistry. The new KIDA database is a unique open tool in which to incorporate modern experiments and calculations performed in the field.

Laboratory measurements on all the possible reactions is clearly a very hard task even if sensitivity analysis (Wakelam et al. 2006) may reduce the number of "key" reactions that are really meaningful. To address this problem statistical theory is commonly used to predict branching ratios (BR) in the outgoing reaction channels of type $A+B \rightarrow C+D$ (Herbst 1978; Liu & Anderson 2005). In databases, if no detailed measurement or calculation exists, zero order statistical predictions are used which is equivalent to put all the reaction in the most exoergic channel.

In the present work, we propose a semi empirical statistical model to go beyond this zero order approximation. This new approach uses the mass spectrometry concept of breakdown curves (Vékey 1996) and a large set of experimental branching ratios (BR) measured in high velocity collisions (HVC) at the Orsay Tandem facility. It is presented in section two. We apply this model to all reactions mediated by an intermediate complex ($A + B \rightarrow AB^*$) such as $C_n^{(0,+)}$, $C_nH^{(0,+)}$, $C_3H_2^{(0,+)}$. With respect to previous work on the same systems (Chabot et al. 2010b) the present model is able to introduce the proper energy deposit associated to a particular reaction. Then it allows to treat not only photodissociation and electronic dissociative recombination (DR) as previously published (Chabot et al. 2010b) but also chemical reactions. In the third section, the BRs predicted by the model are presented and

compared with the BRs from KIDA¹, OSU 01-2007² and UdFA06³ databases for DR, ion-neutral, neutral - neutral, and anion-cation molecular reactions. In the fourth section, effects of the new BRs on the gas-phase chemistry are studied in the dark Taurus Molecular Cloud 1 (TMC1) conditions (Toelle et al. 1981) and in the photon-dominated region (PDR) Horsehead Nebula conditions (Pety et al. 2005).

2. Semi empirical statistical model

2.1. Principle

In a statistical microcanonical formulation of the fragmentation (Martinet et al. 2004), the branching ratio of a decaying channel j may be written:

$$BR_j = \int_0^{+\infty} BDC_j(E) \times f(E) dE \quad (1)$$

Where $f(E)$ is the normalized internal energy distribution of the parent that undergoes fragmentation and $BDC_j(E)$ is the internal-energy dependent dissociation probability, also called breakdown curve for channel j , verifying at each energy:

$$\sum_j BDC_j(E) = 1 \quad (2)$$

The principle of our model is the following: since we measure, in experiments, fragmentation branching ratios BR_j for all channels, de-exciting a molecule whose internal energy distribution $f(E)$ is known (Tuna et al. 2008; Chabot et al. 2010b), we extract the $BDC_j(E)$ for all j channels, by equation (1) inversion. These $BDC_j(E)$ can then be used to predict BRs in a molecule possessing any internal energy, using equation (1), that means, for a variety of physical or chemical processes associated to very different energy deposits as will be shown. The concept of breakdown curves, or breakdown diagram, is well known in mass spectrometry (see for instance Vékey (1996)) and has been recently used for theoretical interpretation of fragmentation branching ratios of neutral (Martinet et al. 2004) or multi-charged (Chabot et al. 2010a) carbon clusters. In figure 1 an example of breakdown curves calculated within the microcanonical metropolis monte carlo (MMMC) method for the

¹<http://kida.obs.u-bordeaux1.fr/>

²<https://www.physics.ohio-state.edu/~eric/research.html>

³<http://www.udfa.net/>

case of C_7 fragmentation is shown (Martinet et al. 2004). This work uses an extensive phase space and extract density of states on the basis of high precision level *ab initio* calculations (Díaz-Tendero et al. 2005). In figure 1, these MMMC BDCs are compared to BDCs derived with the present model by inversion of equation (1) and using a physical parametrization of $BDC_j(E)$ as detailed below. Both approaches give very similar results.

2.2. Construction of the breakdown curves

The energy dependence of $BDC_j(E)$ is easily understandable. When the parent internal energy is below the energy needed for the channel j to occur, the probability is zero. When the energy is above the energy needed for *additional* dissociation of the daughter or of one of the fragments, the probability of channel j is decreasing rapidly to zero. Between the two, the probability is either 1 if this dissociation channel is unique or less than one if there is competition with other dissociation channels. Accordingly, we expressed the $BDC_j(E)$ curve as follows:

$$BDC_j(E) = \frac{a_j \times G_j(E)}{\sum_j a_j \times G_j(E)} \quad (3)$$

where $G_j(E)$ has the generic form depicted in figure 2, a_j takes into account the possible competition of channel j with other opened channels and the denominator ensures normalization (2).

The physical interpretation of $G_j(E)$ is the following: it represents the probability of dissociation along channel j when not in competition with another channels with the same number of fragments. The rise above E_{dis} and the decrease above E_{disap} of $G_j(E)$ (see figure 2) are due to the competition with channel having a different number of fragments. The rise and decrease of the $G_j(E)$ function are usually steep which can be easily explained. Indeed, Vékey (1996) has shown that the ratio between probabilities of competitive channels is equal, at infinite times, to the ratio between corresponding rate constants and it is well known that rate constants (and their ratios) do vary rapidly at the opening (or closing) of a channel⁴ whereas ratios tend to be energy independent elsewhere.

⁴Expression of the rate constant for dimer and trimer evaporation from a cluster having internal energy below or above the opening of further dimer and trimer dissociation may be found for instance in Díaz-Tendero et al. (2005) (equations (31) and (35)).

The $G_j(E)$ function depends apparently on four parameters: E_{dis} , E_{sat} , E_{disap} , and E_{end} . In fact, the decrease of $G_j(E)$ is complementary to the increase of the daughter fragmentation channel, as mentioned before. It makes E_{disap} to be equal to the lowest E_{dis} of the daughter fragment and E_{end} to be equal to the corresponding E_{sat} . We are then left with the determination of E_{dis} and E_{sat} for a particular dissociation channel. E_{dis} corresponds to the minimum energy needed for this channel to occur, i.e, the dissociation (or formation) energy that is usually known from literature (see §2-3). The E_{sat} value and the variation between E_{dis} and E_{sat} is more difficult to evaluate. The competition between channels with a different number of emitted fragments is explained by the different partitioning of the parent internal energy. Indeed, this energy may be used for production, motion and internal excitation of the fragments. We used MMMC breakdown curves as a guide to estimate E_{sat} values. From this theoretical work (Díaz-Tendero et al. 2006a) we could deduce that:

$$E_{sat} \approx E_{dis} + 1.0eV \quad \text{if } N_F = 2 \quad (4)$$

$$E_{sat} \approx E_{dis} + (N_F - 2) \times 1.5eV \quad \text{if } N_F > 2 \quad (5)$$

where N_F is the number of emitted fragments in the considered channel. Dispersion of $E_{sat}-E_{dis}$ values from channel to channel was found of the order of 25%.

On the other hand, the slope of the curve between E_{dis} and E_{sat} was modelled by the following function:

$$G_j = \frac{1}{2} \times (1 - \cos(\pi \times \frac{E_{dis} - E}{E_{sat} - E_{dis}})) \quad (6)$$

Having constructed the $G_j(E)$, the a_j scaling factors were extracted by minimization between measured and predicted BRs using equation (1)(2) and (3). By this manner semi empirical BDC s were obtained.

2.3. Model inputs

We used dissociation energies for C_n and C_n^+ taken from Díaz-Tendero et al. (2006a) and Díaz-Tendero et al. (2006b). They have applied the density functional theory (DFT) with the B3LYP functional for exchange and correlation. For C_nH we used dissociation energies of Pan et al. (2003) and for C_3H_2 those of Mebel et al. (1998). For dissociation energies of C_nH^+

and $C_3H_2^+$ species we combined those last neutral dissociation energies with the ionisation potentials from Clauberg et al. (1992).

The set of experimental BRs that we used to adjust the scaling factors a_j in the model were obtained with HVC experiments. Part of them has already been published in Tuna et al. (2008) (Tables II to V: C_nH ; Tables VII to X: C_nH^+ $n=1, 4$) and in Chabot et al. (2006) (Tables 1 to 10: C_n , $n=2, 10$). All other unpublished experimental BRs concerning C_n^+ , C_3H_2 and $C_3H_2^+$ are given in supplementary material available online. Details on the measurements for those last species may be found in Chabot et al. (2006) and in Tuna et al. (2008).

Determination of the internal energy distribution resulting from the high velocity collision, $f(E)$, was done using multiplicity (i.e probability distribution in numbers of fragments) as detailed in Tuna et al. (2008) and Díaz-Tendero et al. (2006a). This is an improvement over the so called thermometer-method (Wysocki et al. 1987) currently used in mass spectrometry.

2.4. Model confidence and error generation

For chemical reactions, the model does not take into account any rule other than the energy conservation. We checked (see appendix A) whether symmetry considerations or spin and angular momentum conservation rules could lead to forbidden transitions of energetically allowed chemical reactions. In Tables of section 3, we indicated the channels where problems may arise. The characteristics of the ground states of reactants and products are given in Table 1.

Measured BRs used in equation (1) (left-hand side) have their own error bars that are almost identically retrieved in BRs predictions. These errors are typically, in absolute, less than 0.03 for C_n species, less than 0.05 for C_nH species and close to 0.10 for a few channels in the case of C_3H_2 measurements. On the other hand, the sensitivity of the model to the used dissociation energies and E_{sat} values was checked. For dissociation energies, we run calculations with either DFT-B3LYP or CCSDT energies (Diaz-Tendero 2005), those typically differ by 1 eV in absolute and by less than 0.1 eV in relative. Changes on predicted BRs have been found to be less than 0.05 in absolute in the worse cases. For E_{sat} , we solved the inversion of equation (1) by introducing a gaussian distribution of $(E_{sat}-E_{dis})$ values with a standard deviation taken equal to 25 % of the peak value.

Figure 3 presents an example of BR distributions that were obtained for C_7 fragmentation and from which error bars were derived. In Tables of section 3 we give these errors for all channels. In the end, the sum of all sources of errors makes the model more a qualitative tool designed to correct unrealistic predictions sometimes present in astrochemical databases (see §3) than a precise quantitative ones.

3. Branching ratios model predictions

3.1. Dissociative recombination

Branching ratios for dissociative recombination (DR) may be predicted with the model assuming that the internal energy of the neutral intermediate complex is equal to its first ionization potential (IP). Calculated BRs with this assumption are reported for C_n^+ , C_nH^+ and $C_3H_2^+$ species in Tables 2, 3 and 4 respectively. In the same tables, BRs found in the most commonly used databases in astrochemistry are reported. We also report the exothermicity in all the outgoing channels.

For C_n^+ and C_3H^+ , since IPs are lower than the lowest energy of three fragment dissociation, only two fragment dissociation channels have to be considered. The model results are very close to previous published BRs (Chabot et al. 2010b), that have been included in the KIDA database. These values differ strongly from predictions of other databases, which clearly underestimate channels with the magical C_3 fragment. For C_4^+ , all databases report the measurements from Heber et al. (2006) and the model is in good agreement with those values.

For the DR of C_2H^+ and C_4H^+ molecules, due to high values of IPs, three fragment channels are open. The model predictions for C_2H^+ are close to the experimental results of Ehlerding et al. (2004). The model confirms the observed but unquantified three fragment channel in experiments by Angelova et al. (2004) for C_4H^+ . Note that in all cases the errors on the predicted BRs for the three fragment channels are quite large. It is because the IP lies just above the opening of the three fragment channels.

The C_3H_2 molecule has two isomers in astrochemistry databases. One is cyclic and the other is linear. Since these two forms differ in formation energy by only 0.1 eV (Tuna 2008), the dissociation energies used in the model were considered to be identical. Note that the C_3/H_2 channel has a formation barrier (Leonori et al. 2008) and we used it as the dissociation

energy in the model. In contrast with formation energies, IPs are quite different between linear and cyclic forms. As can be seen in Table 4, DR- BR are not identical for the two isomers. For the linear form, three fragment channels are predicted to be more populated. Note that the errors on the model are quite large in both cases because internal energies are close to the opening energies of the three fragment channels.

3.2. Ion-molecule reactions

3.2.1. Charge exchange reaction with He^+

Exothermic charge exchange reaction between molecules and He^+ occurs with large reaction rates, as some electronic states in the inner valence shells of the molecule are energetically close to the Helium IP (Fisher et al. 1990). This makes the charge transfer resonant. Since in the output channel, He atom is likely to be produced with only little kinetic energy, the internal energy of the neutral molecule is assumed to be close to $\Delta IP = IP(He) - IP(\text{molecule})$. Tables 5, 6, and 7 give the BRs calculated by the model for C_n , C_nH and C_3H_2 charge exchange with He^+ . Internal energies reported in the same tables were obtained using the IPs reported in Tables 2, 3, and 4 with $IP(He)=24.58$ eV.

In all the cases, because the IP of helium is high, the internal energy of the charged molecule is also high. As a consequence, fragmentation into three fragments operates, although neglected in all databases. For C_4 , it is small, but it increases with the size and reaches half of the probability for C_{10} . Nevertheless ΔIP s are close to the dissociation energies of three fragment channels, therefore errors are quite important. For example for C_6 species, using CCSDT calculations for dissociation energies instead of DFT-B3LYP (Diaz-Tendero 2005), we find that almost all the dissociation goes into three fragment channels. Here again, all reported BRs in databases miss the importance of the channels with a C_3 emission. For the C_nH , the three fragment channel contribution is also increasing with the size and reaches almost 100% for C_4H . Differences between the model predictions and the values reported in databases are huge. It is because in databases: (i) only two fragment channels are considered and (ii) the H emission is strongly overestimated.

Since in databases cyclic and linear isomers of C_3H are separated, we report BRs using the same dissociation energies but a different IP for the linear and cyclic species. As a consequence, the linear species produces

more three fragment channels than the cyclic one. For C_3H_2 , all the probability goes into the three fragment channels.

3.2.2. Ion neutral bimolecular reactions

For bimolecular reactions between neutral and ionic species, the internal energy of the intermediate complex results from the association. Therefore it is calculated by the dissociation energy of the reverse pathway. For instance for $C_n + C^+$ reaction, the internal energy of the complex (E_{ass}) is equal to the dissociation energy of C_{n+1}^+ into $C_n + C^+$. Tables 8 to 13 give the BR calculated by the model for intermediate complexes of type C_n^+ , C_nH^+ and $C_3H_2^+$.

For the reactions between C_n species and C^+ displayed in Table 8, the radiative deexcitation channel is always the only output channel in the reported databases. This is true for $C_3 + C^+$ since in that case internal energy in the intermediate complex C_4^+ is below all the energies of dissociation. For all other $C_n + C^+$ reactions, the internal energy in the intermediate complex is above dissociation energy and those dissociation channels must be considered. The lifetime of an intermediate complex is related to the energy difference between the internal energy and the dissociation energy. If the energy is close to the threshold, the complex will survive and will emit photons. While, if the energy is well above threshold it undergoes fragmentation. Using Weisskopf calculations (Díaz-Tendero et al. 2005) we showed that, for C_n^+ , fragmentation occurs faster than $10\mu s/100\mu s$ for a few tenths of eV above threshold (Diaz-Tendero 2005). Whereas photon emission is on the millisecond time scale (Parneix P., private communication). Then, for all reactions presented in Table 8 fragmentation dominates, which is in strong disagreement with databases assumptions.

For the $C_2H_2 + C^+$ reaction (Table 9), the model agrees with experiments of Anicich et al. (1986).

Concerning the reactions with H^+ (Table 10), two channels have a very low exothermicity (< 0.2 eV). For those two, model results are very uncertain. It is noticeable that for $C_4 + H^+$ reaction, charge transfer is not the dominant channel.

Looking at Table 11, it appears that many of the reactions $C_n + C_2^+$ are not implemented in databases. Pseudo time dependant chemical models for dense clouds (Herbst & Leung 1986) predict similar abundances for C_2 and C_3 . Similarly, C_3^+ and C_4^+ would

have abundances close to C_2^+ . Thus reactions between C, C_2 and C_3 with C_3^+ or C_4^+ may be important to include into the models. The same remark holds for the reactions of C_2H , C_3H with C_2^+ , C_3^+ , C_4^+ , which are not implemented either.

For the reaction of $C_2H + CH^+$ (Table 12), H_2 production predicted by the model is small due to the energy barrier as mentioned previously.

3.3. Neutral-neutral reactions

For neutral - neutral reactions, as in the case of ion-neutral reactions, internal energy of the intermediate complex (E_{ass}) is given by the dissociation energy of the reverse pathway. Tables 14 and 15 give the model BRs for the C_nH_m intermediate complexes together with database BRs and exothermicities. The agreement between model predictions and reported values from KIDA and OSU databases is pretty good due to a recent update based on statistical calculations (Wakelam et al. 2009). The $C + C_2H_2$ reaction (Table 14) has been extensively studied both experimentally and theoretically (Costes et al. 2009, and references therein). The BR of the C_3/H_2 channel has been found to be strongly related to the collisional energy. At 0K (values reported in table 13), the BR is large (0.73) and it decreases down to 0.2 above 50 K. The model fails to reproduce the values at 0K and the temperature dependence. Note that this reaction is complicated, involving both a barrier on the outgoing C_3/H_2 channel and a intersystem crossing between triplet and singlet state of the intermediate complex (Leonori et al. 2008).

3.4. Ion-ion reactions

For ion pair recombinations of type $A^+ + B^- \rightarrow (AB)^* \rightarrow C + D$, internal energy of the intermediate complex that undergoes fragmentation is given by : $E_{dis}^{A/B} + IP^A - EA^B$, with $E_{dis}^{A/B}$, the energy of dissociation of AB into A/B, IP^A : the ionization potential of the fragment A and EA^B : the electron affinity of the fragment B. Table 16 gives the model BRs for C_nH_m intermediate complexes. These reactions are so far not implemented into the UDfA database. Internal energy of all intermediate complexes are very high and three fragment channels are dominating for all sizes. Values reported in databases have clearly to be re-evaluated.

4. Application to ISM chemistry

Effects of the new branching ratios were studied using chemical models for two different environments: dark clouds and photon-dominated regions.

4.1. Dark clouds

To compute the chemical composition of a dark cloud, we used the Nautilus gas-grain model (Hersant et al. 2009). This code takes into account the gas-phase chemistry, the sticking of gas-phase species to the surface, the evaporation of species from the surface and the surface reactions using the rate equation approximation. Details on these processes are given in Semenov et al. (2010). Species are initially in the atomic form, except hydrogen which is molecular. The elemental abundances are those of Daranlot et al. (2012). The cloud temperature (gas and dust) is 10 K, the H density is $2 \times 10^4 \text{ cm}^{-3}$, the cosmic-ray ionization rate is $1.3 \times 10^{-17} \text{ s}^{-1}$ and the visual extinction is 30. The gas-phase reactions are based on the kida.uva.2011 network (Wakelam et al. 2012) while the surface network is the same as Garrod et al. (2007). In the gas-phase network, we have modified the branching ratios according to the new values listed in Tables 2 to 16. BRs for which the KIDA values have been underlined correspond to experimental results that were kept in the analysis i.e. not replaced by the model values.

Effects of the new BRs are illustrated in Fig. 4 for three selected species. These molecules have been chosen because they present the largest differences in the abundances computed with the two networks. The effect on the chemistry of dark clouds is mainly seen at early times i.e. before 2×10^4 yr. It is because later on, hydrocarbon chemistry is occurring at the surface of grains and through negative species reactions. The early formation of carbon chains, such as C_n and HC_nN , are delayed with the new BRs. As a consequence, for few species produced at the end of reaction chains with hydrocarbon, large delays are obtained and peculiar old/new ratio shapes obtained. It is for instance the case of the CH_3CHO molecule populated from the C_2H_5 precursor through $C_2H_5 + O \rightarrow H + CH_3CHO$ chemical reaction (see left of Fig. 4).

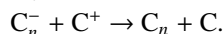
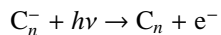
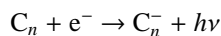
4.2. Photon-dominated regions

For photon-dominated regions modeling, we used the Meudon PDR code (<http://pdr.obspm.fr>, Le Petit et al. 2006). The Meudon PDR code consistently solves

the radiative transfer from far UV to sub-millimeter, chemistry, and thermal balance in a 1D plan-parallel and stationary slab of dust and gas. The density and thermal structures were determined in a consistent way using a constant $4 \times 10^6 \text{ K cm}^{-3}$ value for pressure (Habart et al. 2005). The intensity of the incident UV flux was set to 60 times the ISRF (in Draine units (Draine 1978)) (Habart et al. 2005), and the cosmic ray flux used was 5×10^{-17} per H and per second (Goicoechea et al. 2009). The initial abundances were those of Goicoechea et al. (2006). These values correspond to the Horsehead Nebula. This object is used for a benchmark calculation since it is well known that within it, the PAH or/and carbon grain reservoir are believed to be the main production source of hydrocarbons (Pety et al. 2005, 2012).

The gas-phase chemistry is identical to the kida.uva.2011 network and, as for dense clouds, the new branching ratios listed in Tables 2 to 16 have been introduced.

Figures 5, 6, and 7 show, as a function of the visual extinction A_v , the ratio of abundances computed with the new branching ratios over the ones computed with the old branching ratios for a selection of species. The figure 5 focuses on some of the large hydrocarbon molecules. Inside the cloud ($A_v > 3$) effects are very small. It is due to the fact that the large anion-neutral reactions, not modified in the present work, are the main pathways for the growth of large carbon chains (Millar et al. 2007). On the contrary, at the edge of the PDR a large effect is observed and species abundances are strongly decreased by the new BRs. It is because in the old network C_n species are locked in a loop that conserves the mass, this is :



With the new BRs (see Table 16) the rates of reactions $C_n^- + C^+ \rightarrow C_n + C$ are put to zero and C_n s are fragmented. Therefore C_n s abundances decrease.

Figure 6 presents the effect of the new branching ratios for small hydrocarbon molecules observed in the real Horsehead Nebula PDR (Teyssier et al. 2004; Pety et al. 2005, 2012). These species are moderately affected by the new branching ratios. Ion-neutral reactions dominate the chemistry of these species together with dissociative recombination. In the Tables 9 to 12, for small size hydrocarbons, the old and the new BRs have only few differences.

Figure 7 presents the effect of the new branching ratios for the other most affected small species. It is noticeable that all contain oxygen. They all derive from the production of O^+ resulting from charge exchange between O and H^+ . With the old network H^+ is produced by cosmic rays and their induced photons while with the new network $CH + C^+ \rightarrow C_2 + H^+$ is a new pathway. As a result H^+ abundance is enhanced and consequently the O^+ chemistry. The error on branching ratio of this particular reaction is quite large and therefore deserves further study.

5. Conclusions

We introduced a statistical model to calculate semi empirical branching ratios based on high velocity collision experiments. We applied the model to many reactions leading to an intermediate excited complex of the type of C_n^{+0} , C_nH^{+0} , and $C_3H_2^{+0}$ that undergoes dissociation. We compared these new branching ratios to the ones from the most popular astrochemical databases. The new semi empirical branching ratios agree quite well with experimental BRs reported in databases with the notable exception of the $C + C_2H_2$ reaction at very low temperature where the model clearly failed. Since most of the BRs in the databases have been obtained with a statistical zero order hypothesis (i.e. all the reaction goes in the most exoergic channel), we propose to replace them by the new semi-empirical BRs which are by far more realistic. We observed the effect of these new branching ratios in a time dependant chemical model under the physical condition of the dark cold cloud TMC1. No modification was found in the calculated abundances in the range of the 10^5 yr and more. On the contrary PDR calculations in the condition of the Horsehead Nebula for low A_v extinction ($A_v < 2$) with the same new branching ratios exhibit notable differences. It concerns hydrocarbon synthesis but also species initiated by reactions with the H^+ ion such as oxygen based molecules. The new network will be available on the KIDA web site⁵.

All persons having worked in AGAT collaboration over the years are indebted for their valuable help in measurements. P. Pernot, P. Parneix and S. Diaz-Tendero are thanked for fruitful discussions. M. Eller is thanked for his careful reading of the manuscript.

⁵<http://kida.obs.u-bordeaux1.fr/>

CNRS-IN2P3, CNRS-INSU, University of Paris-Sud have been the contributing partners. VW's research is funded by the French national program PCMI and the Observatoire Aquitain des Sciences de l'Univers. P. Gratier is funded by the grant ANR-09-BLAN-0231-01 from the French *Agence Nationale de la Recherche* as part of the SCHISM project (<http://schism.ens.fr/>).

A. Appendix A. Experimental high velocity collision branching ratios

The measured BRs for C_n^+ , C_3H_2 , and $C_3H_2^+$ are displayed in Tables 17 to 23, Table 24 and Table 25 respectively. All details concerning the experiments may be found in Chabot et al. (2006) and Tuna et al. (2008).

B. Appendix B. Correlation rules in chemical reactions

We examine in this appendix whether chemical reactions between reactants X and Y in their electronic ground states leading to products Z and T in their electronic ground states are possible on the basis of correlation rules. These correlation rules, derived on the assumption of an adiabatic change of internuclear distances and in the frame of the Russell-Saunders coupling (Herzberg & Spinks 1939), have three origins:

i) Spin conservation

From the spin conservation and spin addition rules there must exist, for the reaction to proceed, one value of the total spin S verifying both conditions:

$$|S(X) - S(Y)| \leq S \leq S(X) + S(Y)$$

$$|S(Z) - S(T)| \leq S \leq S(Z) + S(T)$$

When this rule is not satisfied the reaction is spin-forbidden and preceded, in Tables 8 to 16, by the sign †. The reaction may nevertheless occur through intersystem crossing.

ii) Angular momentum conservation (linear molecules)

For linear molecules, similar rules hold for the projection, along the internuclear axis, of the angular momentum. For the reaction to proceed there must exist one projection of the total angular momentum M_l such as:

$$M_l = |M_l(X) + M_l(Y)| = |M_l(Z) + M_l(T)|$$

Where $M_l(X)$ is taking values between $-l_X$ to $+l_X$ if X is an atom in a state of angular momentum l_X and is equal to $\pm\Lambda$ if X is a molecule in a state characterized by the Λ quantum number ($\Lambda = 0, 1, 2, \dots$ for $\Sigma, \Pi, \Delta, \dots$ states). When this rule is not satisfied the reaction is preceded, in Tables 8 to 16, by the sign §.

iii) Symmetry considerations

Symmetry properties of atoms and molecules play an important role in the association or dissociation of molecular complexes. In the framework of the group theory it is possible to predict if the reaction is allowed or not. We did that, using the correlation Tables of Herzberg (1966) and Carter (1997). When symmetry rules avoid the reaction, this one is preceded, in Tables 8 to 16, by the sign \diamond .

In Table 1 a list of all atoms, molecules and clusters participating to the chemical reactions studied in the present work together with their electronic ground states and symmetry point groups is given. References are Díaz-Tendero et al. (2005) for C_n , Díaz-Tendero (2005) for C_n^+ , Szczepanski et al. (1997) for C_n^- , Tuna et al. (2008) for C_nH et C_nH^+ and the KIDA database for C_3H_2 and $C_3H_2^+$.

REFERENCES

- Alexander, C. M. O. ., Fogel, M., Yabuta, H., & Cody, G. D. 2007, *Geochim. Cosmochim. Acta*, 71, 4380
- Allamandola, L. J., Bernstein, M. P., Sandford, S. A., & Walker, R. L. 1999, *Space Sci. Rev.*, 90, 219
- Angelova, G., Novotny, O., Mitchell, J. B. A., Rebrion-Rowe, C., Garrec, J. L. L., Bluhme, H., Seiersen, K., & Andersen, L. H. 2004, *International Journal of Mass Spectrometry*, 232, 195
- Anicich, V. G., Huntress, W. T., & McEwan, M. J. 1986, *The Journal of Physical Chemistry*, 90, 2446
- Carter, R. 1997, *Molecular Symmetry and Group Theory* (Wiley)
- Chabot, M., Martinet, G., Mezdari, F., Diaz-Tendero, S., Béroff-Wohrer, K., Désesquelles, P., Della-Negra, S., Hamrita, H., LePadellec, A., Tuna, T., Montagnon, L., Barat, M., Simon, M., & Ismail, I. 2006, *Journal of Physics B Atomic Molecular Physics*, 39, 2593
- Chabot, M., Mezdari, F., Béroff, K., Martinet, G., & Hervieux, P.-A. 2010a, *Physical Review Letters*, 104, 043401
- Chabot, M., Tuna, T., Béroff, K., Pino, T., Le Padellec, A., Désesquelles, P., Martinet, G., Nguyen-Thi, V. O., Carpentier, Y., Le Petit, F., Roueff, E., & Wakelam, V. 2010b, *A&A*, 524, A39
- Clauberg, H., Minsek, D., & Chen, P. 1992, *Journal of the American Chemical Society*, 114, 99
- Clayton, D. 2003, *Handbook of Isotopes in the Cosmos: Hydrogen to Gallium, Handbook of Isotopes in the Cosmos* (Cambridge University Press)
- Costes, M., Halvick, P., Hickson, K. M., Daugey, N., & Naulin, C. 2009, *ApJ*, 703, 1179
- Dame, T. M., Hartmann, D., & Thaddeus, P. 2001, *ApJ*, 547, 792
- Daranlot, J., Hincelin, U., Bergeat, A., Costes, M., Loison, J.-C., Wakelam, V., & Hickson, K. M. 2012, *Proceedings of the National Academy of Science*, 109, 10233
- Dartois, E. 2011, in *EAS Publications Series*, Vol. 46, *EAS Publications Series*, ed. C. Joblin & A. G. G. M. Tielens, 381–391
- Díaz-Tendero, S., Hervieux, P.-A., Alcamí, M., & Martín, F. 2005, *Phys. Rev. A*, 71, 033202
- Díaz-Tendero, S., Sánchez, G., Alcamí, M., Martín, F., Hervieux, P. A., Chabot, M., Martinet, G., Désesquelles, P., Mezdari, F., Wohrer-Béroff, K., Negra, S. D., Hamrita, H., Lepadellec, A., & Montagnon, L. 2006a, *International Journal of Mass Spectrometry*, 252, 126
- Díaz-Tendero, S., Sánchez, G., Hervieux, P.-A., Alcamí, M., & Martín, F. 2006b, *Brazilian Journal of Physics*, 36, 529
- Díaz-Tendero, V. 2005, PhD thesis, University Autónoma de Madrid, unpublished
- Draine, B. T. 1978, *ApJS*, 36, 595
- Ehlerding, A., Hellberg, F., Thomas, R., Kalhori, S., Viggiano, A. A., Arnold, S. T., Larsson, M., & Af Ugglas, M. 2004, *Physical Chemistry Chemical Physics (Incorporating Faraday Transactions)*, 6, 949
- Fisher, E. R., Weber, M. E., & Armentrout, P. B. 1990, *The Journal of Chemical Physics*, 92, 2296
- Garrod, R. T. & Herbst, E. 2006, *A&A*, 457, 927
- Garrod, R. T., Wakelam, V., & Herbst, E. 2007, *A&A*, 467, 1103
- Godard, M., Féraud, G., Chabot, M., Carpentier, Y., Pino, T., Brunetto, R., Duprat, J., Engrand, C., Bréchnignac, P., D’Hendecourt, L., & Dartois, E. 2011, *A&A*, 529, A146
- Goicoechea, J. R., Pety, J., Gerin, M., Hily-Blant, P., & Le Bourlot, J. 2009, *A&A*, 498, 771
- Goicoechea, J. R., Pety, J., Gerin, M., Teyssier, D., Roueff, E., Hily-Blant, P., & Baek, S. 2006, *A&A*, 456, 565
- Habart, E., Abergel, A., Walmsley, C. M., Teyssier, D., & Pety, J. 2005, *A&A*, 437, 177
- Heber, O., Seiersen, K., Bluhme, H., Svendsen, A., Andersen, L. H., & Maunoury, L. 2006, *Physical Review A (Atomic, Molecular, and Optical Physics)*, 73, 022712
- Herbst, E. 1978, *ApJ*, 222, 508
- Herbst, E. & Leung, C. M. 1986, *MNRAS*, 222, 689

- Hersant, F., Wakelam, V., Dutrey, A., Guilloteau, S., & Herbst, E. 2009, *A&A*, 493, L49
- Herzberg, G. 1966, *Molecular spectra and molecular structure. Vol.3: Electronic spectra and electronic structure of polyatomic molecules*
- Herzberg, G. & Spinks, J. 1939, *Molecular Spectra and Molecular Structure: Electronic spectra and electronic structure of polyatomic molecules*, Prentice-Hall physics series (Prentice-Hall)
- Jones, A. P., Duley, W. W., & Williams, D. A. 1990, *QJRAS*, 31, 567
- Le Petit, F., Nehmé, C., Le Bourlot, J., & Roueff, E. 2006, *ApJ*, 164, 506
- Leonori, F., Petrucci, R., Hickson, K. M., Segoloni, E., Balucani, N., Le Picard, S. D., Foggi, P., & Casavecchia, P. 2008, *Planet. Space Sci.*, 56, 1658
- Leonori, F., Petrucci, R., Segoloni, E., Bergeat, A., Hickson, K. M., Balucani, N., & Casavecchia, P. 2008, *The Journal of Physical Chemistry A*, 112, 1363
- Liu, J. & Anderson, S. L. 2005, *International Journal of Mass Spectrometry*, 241, 173
- Martinet, G., Díaz-Tendero, S., Chabot, M., Wohrer, K., Negra, S. D., Mezdari, F., Hamrita, H., Désesquelles, P., Padellec, A. L., Gardés, D., Lavergne, L., Lalu, G., Grave, X., Clavelin, J. F., Hervieux, P., Alcamí, M., & Martín, F. 2004, *Physical Review Letters*, 93, 063401
- Matsuura, M., Barlow, M. J., Zijlstra, A. A., Whitelock, P. A., Cioni, M.-R. L., Groenewegen, M. A. T., Volk, K., Kemper, F., Kodama, T., Lagarde, E., Meixner, M., Sloan, G. C., & Srinivasan, S. 2009, *MNRAS*, 396, 918
- McElroy, D., Walsh, C., Markwick, A. J., Cordiner, M. A., Smith, K., & Millar, T. J. 2013, *A&A*, 550, A36
- Mebel, A., Jackson, W., Chang, A., & Lin, S. 1998, *Journal of the american chemical society*, 120, 5751
- Millar, T. J., Walsh, C., Cordiner, M. A., Ní Chuimín, R., & Herbst, E. 2007, *ApJ*, 662, L87
- Pan, L., Rao, B. K., Gupta, A. K., Das, G. P., & Ayyub, P. 2003, *J. Chem. Phys.*, 119, 7705
- Pety, J., Gratier, P., Guzmán, V., Roueff, E., Gerin, M., Goicoechea, J. R., Bardeau, S., Sievers, A., Le Petit, F., Le Bourlot, J., Belloche, A., & Talbi, D. 2012, *A&A*, 548, A68
- Pety, J., Teyssier, D., Fossé, D., Gerin, M., Roueff, E., Abergel, A., Habart, E., & Cernicharo, J. 2005, *A&A*, 435, 885
- Prasad, S. S. & Huntress, Jr., W. T. 1980, *ApJS*, 43, 1
- Salpeter, E. E. 1952, *ApJ*, 115, 326
- Scott, A., Duley, W. W., & Pinho, G. P. 1997, *ApJ*, 489, L193
- Semenov, D., Hersant, F., Wakelam, V., Dutrey, A., Chapillon, E., Guilloteau, S., Henning, T., Launhardt, R., Piétu, V., & Schreyer, K. 2010, *A&A*, 522, A42
- Szczepanski, J., Ekern, S., & Vala, M. 1997, *The Journal of Physical Chemistry A*, 101, 1841
- Teyssier, D., Fossé, D., Gerin, M., Pety, J., Abergel, A., & Roueff, E. 2004, *A&A*, 417, 135
- Tielens, A. G. G. M. 2008, *ARA&A*, 46, 289
- Tielens, A. G. G. M., McKee, C. F., Seab, C. G., & Hollenbach, D. J. 1994, *ApJ*, 431, 321
- Tielens, A. G. G. M., Tokunaga, A. T., Geballe, T. R., & Baas, F. 1991, *ApJ*, 381, 181
- Toelle, F., Ungerechts, H., Walmsley, C. M., Winnewisser, G., & Churchwell, E. 1981, *A&A*, 95, 143
- Tuna, T. 2008, PhD thesis, Université Paris Sud, unpublished
- Tuna, T., Chabot, M., Pino, T., Désesquelles, P., Lepadellec, A., Martinet, G., Barat, M., Lucas, B., Mezdari, F., Montagnon, L., van-Oanh, N. T., Lavergne, L., Lachaize, A., Carpentier, Y., & Béroff, K. 2008, *J. Chem. Phys.*, 128, 124312
- Vékey, K. 1996, *Journal of Mass Spectrometry*, 31, 445
- Wakelam, V., Herbst, E., Loison, J.-C., Smith, I. W. M., Chandrasekaran, V., Pavone, B., Adams, N. G., Bacchus-Montabonel, M.-C., Bergeat, A., Béroff, K., Bierbaum, V. M., Chabot, M., Dalgarno, A., van Dishoeck, E. F., Faure, A., Geppert, W. D.,

Gerlich, D., Galli, D., Hébrard, E., Hersant, F.,
Hickson, K. M., Honvault, P., Klippenstein, S. J.,
Le Picard, S., Nyman, G., Pernot, P., Schlemmer,
S., Selsis, F., Sims, I. R., Talbi, D., Tennyson, J.,
Troe, J., Wester, R., & Wiesenfeld, L. 2012, ApJS,
199, 21

Wakelam, V., Herbst, E., & Selsis, F. 2006, A&A, 451,
551

Wakelam, V., Loison, J.-C., Herbst, E., Talbi, D.,
Quan, D., & Caralp, F. 2009, A&A, 495, 513

Woodall, J., Agúndez, M., Markwick-Kemper, A. J.,
& Millar, T. J. 2007, A&A, 466, 1197

Wysocki, V. H., Kenttamaa, H. I., & Cooks, R. 1987,
International Journal of Mass Spectrometry and Ion
Processes, 75, 181

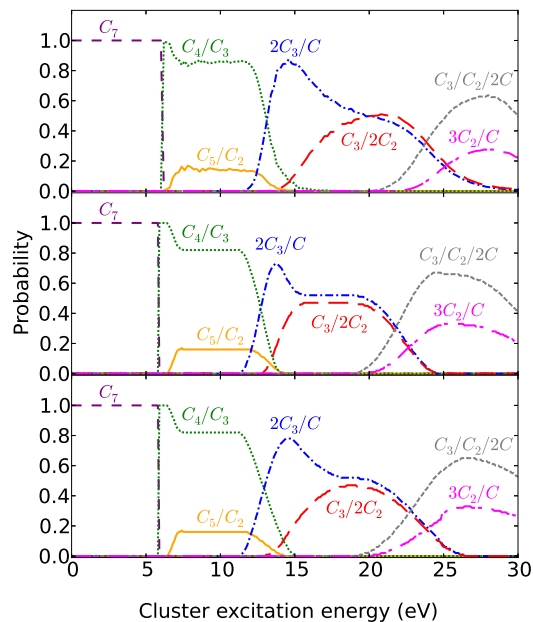


Fig. 1.— Breakdown curves for the C_7 molecule. Upper panel: Theoretical microcanonical metropolis monte carlo (MMMC) calculation (Martinet et al. 2004). Middle panel: semi empirical model with E_{sat} obtained with formulae 4 and 5. Lower panel: semi empirical model with E_{sat} adjusted inside the error bars (see §2.4.) to reproduce MMMC calculations.

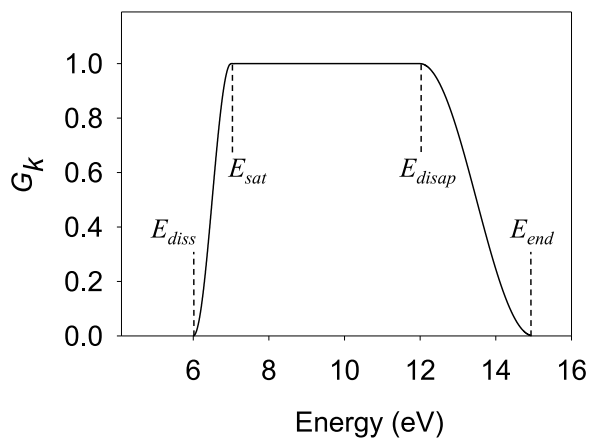


Fig. 2.— Generic form of the G_j function.

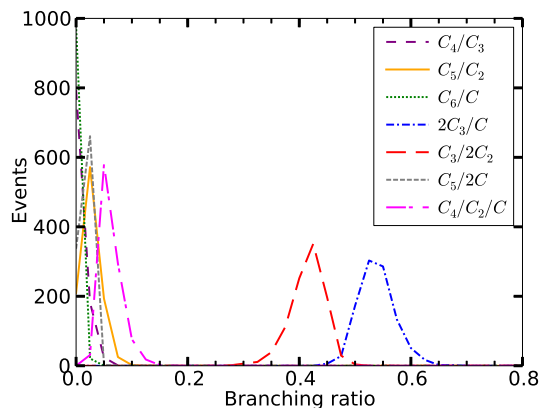


Fig. 3.— Example of BR distributions obtained when introducing the error on $E_{sat} - E_{dis}$ (see § 2.4). Internal energy of the C_7 molecule was taken equal to 13.87 eV in the model.

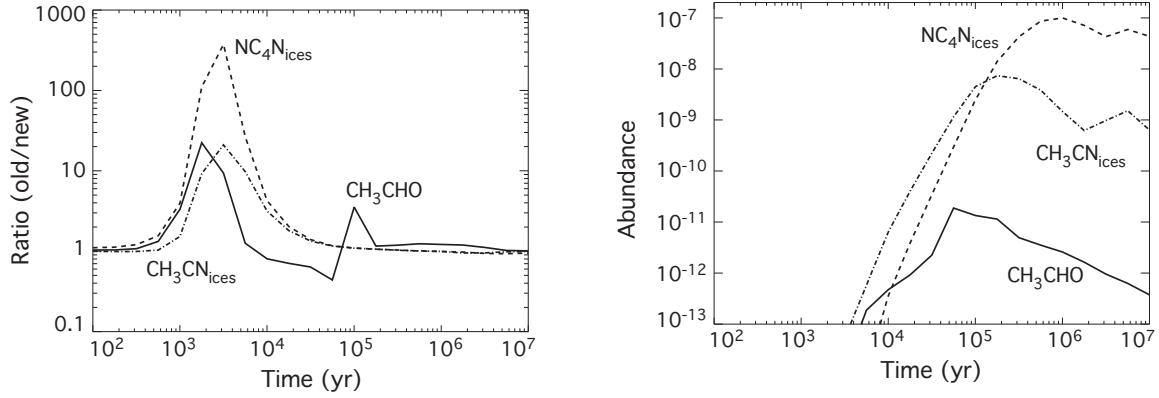


Fig. 4.— Left: ratio between the species abundances computed with the kida.uva.2011 network (old) and the new branching ratios (new) . Right: predicted abundances using the new branching ratios as a function of time are presented for selected species. Calculations are for a dark cloud.

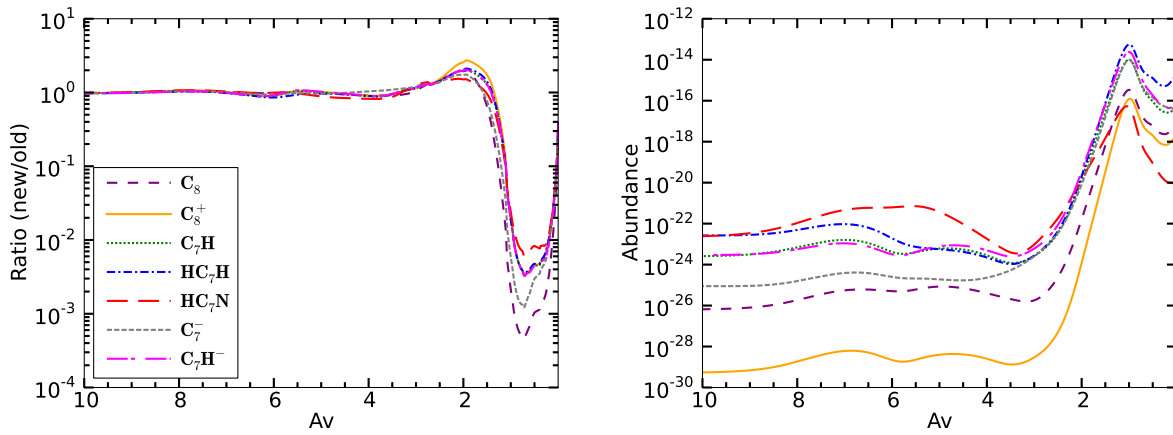


Fig. 5.— Left: ratio between the species abundances computed with the new branching ratios (new) and the kida.uva.2011 network (old). Right: predicted abundances using the new branching ratios as a function of visual attenuation (A_v). Calculations are for a PDR region with conditions similar to those found in the Horsehead Nebula.

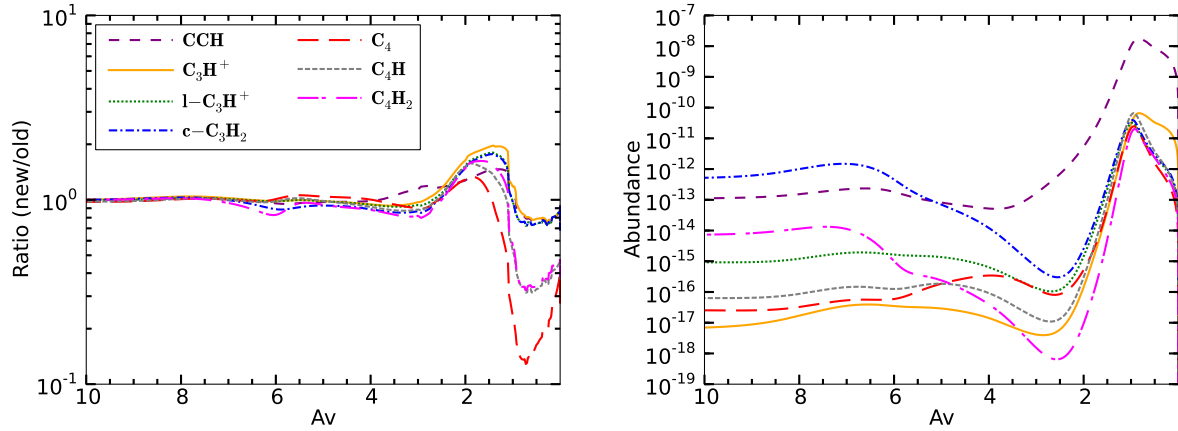


Fig. 6.— Left: ratio between the species abundances computed with the new branching ratios (new) and the kida.uva.2011 network (old). Right: predicted abundances using the new branching ratios as a function of visual attenuation (A_v). Calculations are for a PDR region with conditions similar to those found in the Horsehead Nebula.

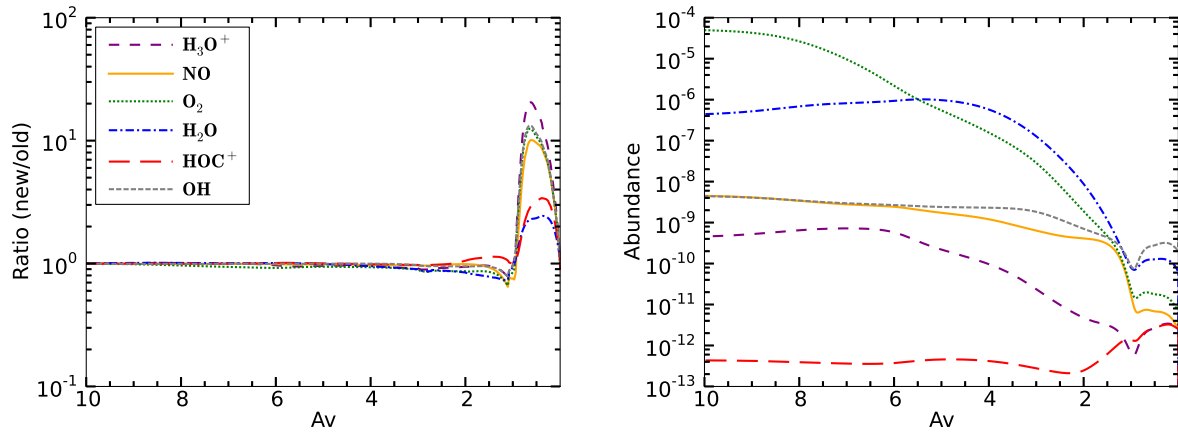


Fig. 7.— Left: ratio between the species abundances computed with the new branching ratios (new) and the kida.uva.2011 network (old). Right: predicted abundances using the new branching ratios as a function of visual attenuation (A_v). Calculations are for a PDR region with conditions similar to those found in the Horsehead Nebula.

Table 1: Electronic ground states (GS) and symmetry point groups (Sym.) of atoms, molecules and clusters participating in chemical reactions studied in the present work.

Species	C	C₂	C₃	C₄	C₅	C₆	C₇	C₈	C₉	C⁺
GS	3P_g	$^1\Sigma_g^+$	$^1\Sigma_g^+$	1A_g	$^1\Sigma_g^+$	$^1A_1'$	$^1\Sigma_g^+$	1A_g	$^1\Sigma_g^+$	2P_u
Sym.	atom	$D_{\infty h}$	$D_{\infty h}$	D_{2h}	$D_{\infty h}$	D_{3h}	$D_{\infty h}$	D_{4h}	$D_{\infty h}$	atom
Species	C₂⁺	C₃⁺	C₄⁺	C₅⁺	C₆⁺	C₇⁺	C₈⁺	C₉⁺	C⁻	C₂⁻
GS	$^4\Sigma_g^-$	2B_2	$^2A'$	$^2\Sigma_u^+$	$^2\Pi_u$	2B_2	2B_u	4A_2	4S_u	$^2\Sigma_g^+$
Sym.	$D_{\infty h}$	C_{2v}	C_s	$D_{\infty h}$	$D_{\infty h}$	C_{2v}	C_{4h}	C_{2v}	atom	$D_{\infty h}$
Species	C₃⁻	C₄⁻	C₅⁻	C₆⁻	C₇⁻	C₈⁻	C₉⁻	CH	C₂H	1-C₃H
GS	$^2\Pi_g$	$^2\Pi_g$	$^2\Pi_u$	$^2\Pi_u$	$^2\Pi_u$	$^2\Pi_g$	$^2\Pi_u$	$^2\Pi$	$^2\Sigma^+$	$^2\Pi$
Sym.	$D_{\infty h}$	$D_{\infty h}$	$D_{\infty h}$	$D_{\infty h}$	$D_{\infty h}$	$D_{\infty h}$	$D_{\infty h}$	$C_{\infty h}$	$C_{\infty h}$	$C_{\infty h}$
Species	c-C₃H	CH⁺	C₂H⁺	C₃H⁺	CH₂	CH₂⁺	C₂H₂	C₂H₂⁺	H	H₂
GS	2B_2	$^1\Sigma^+$	$^3\Pi$	$^1\Sigma^+$	3B_1	2A_1	$^1\Sigma_g^+$	$^2\Pi_u$	2S_g	$^1\Sigma_g^+$
Sym.	C_{2v}	$C_{\infty v}$	$C_{\infty v}$	$C_{\infty v}$	C_{2v}	C_{2v}	$C_{\infty v}$	$C_{\infty h}$	atom	$D_{\infty h}$

Table 2: Branching ratios (BR) for the dissociative electronic recombination (DR) reactions of C_n^+ molecules. BRs predicted by the model are reported in column 2 with in parenthesis part of the estimated errors (see text). KIDA (on Jan. 2012) , OSU 01-2007 and UdFA06 database BRs are given in column 3, 4 and 5 respectively. Underlined BRs are from dedicated experiments and should be used in chemical models. In column 6, ionization potentials (IP) of the C_n complexes are reported in bold, together with in front of each channel exothermicities. All energies are in eV.

Reaction	Model	KIDA	OSU	UdFA	IP / ΔE
$C_4^+ + e^- \rightarrow$					11.5
C_3/C	0.72(\pm 0.02)	<u>0.6</u>	<u>0.6</u>	<u>0.6</u>	6.48
C_2/C_2	0.28 (\pm 0.02)	<u>0.4</u>	<u>0.4</u>	<u>0.4</u>	5.41
$C_5^+ + e^- \rightarrow$					11.0
C_3/C_2	0.84(\pm 0.02)	0.85	0.5	0.5	5.19
C_4/C	0.16(\pm 0.02)	0.15	0.5	0.5	4.03
$C_6^+ + e^- \rightarrow$					9.7
C_3/C_3	0.77(\pm 0.02)	0.8			5.70
C_4/C_2	0.14(\pm 0.02)	0.1	0.5	0.5	3.26
C_5/C	0.09(\pm 0.01)	0.1	0.5	0.5	4.24
$C_7^+ + e^- \rightarrow$					10.1
C_4/C_3	0.79(\pm 0.01)	0.8	0.14	0.14	4.59
C_5/C_2	0.20(\pm 0.01)	0.2	0.43	0.43	4.30
C_6/C	0.01(\pm 0.01)		0.43	0.43	3.77
$C_8^+ + e^- \rightarrow$					9.2
C_5/C_3	0.86(\pm 0.03)	0.8			4.70
C_4/C_4	0.07(\pm 0.02)				2.90
C_6/C_2	0.04(\pm 0.01)	0.2	0.5	0.5	2.67
C_7/C	0.03(\pm 0.01)		0.5	0.5	3.45
$C_9^+ + e^- \rightarrow$					9.4
C_6/C_3	0.62(\pm 0.02)	0.65			3.78
C_5/C_4	0.31(\pm 0.02)	0.3			3.53
C_7/C_2	0.06(\pm 0.01)	0.05	0.5	0.5	3.03
C_8/C	0.01(\pm 0.01)		0.5	0.5	2.70
$C_{10}^+ + e^- \rightarrow$					9.2
C_7/C_3	0.69(\pm 0.02)	0.75			4.4
C_5/C_5	0.27(\pm 0.02)	0.25			4.4
C_6/C_4	0.04(\pm 0.01)				2.9
C_9/C	0.0(\pm 0.01)		0.5	0.5	3.2
C_8/C_2	0.0(\pm 0.01)		0.5	0.5	2.6

Table 3: Branching ratios for the dissociative electronic recombination (DR) reactions of C_nH^+ molecules. Same legends as Table 2.

Reaction	Model	KIDA	OSU	UDfA	$IP / \Delta E$
$C_2H^+ + e^- \rightarrow$					11.6
C_2/H	0.58(\pm 0.05)	<u>0.43</u>	0.43	0.44	6.59
C/CH	0.34(\pm 0.04)	<u>0.39</u>	0.39	0.56	3.74
$C/C/H$	0.08(\pm 0.05)	<u>0.18</u>	0.18		0.1
$C_3H^+ + e^- \rightarrow$					8.7
C_3/H	0.61(\pm 0.02)	0.5	0.5	0.5	5.24
C_2H/C	0.36(\pm 0.02)	0.5	0.5	0.5	2.49
C_2/CH	0.03(\pm 0.01)				1.13
$C_4H^+ + e^- \rightarrow$					12.0
$C_3/C/H$	0.40(\pm 0.12)				1.64
C_2H/C_2	0.22(\pm 0.06)	0.3	0.3		5.39
C_4/H	0.19(\pm 0.08)	0.4	0.4	1.0	7.13
C_3H/C	0.19(\pm 0.09)	0.15	0.15		5.29
C_3/CH	0.0(\pm 0.001)	0.15	0.15		6.90

Table 4: Branching ratios for the dissociative electronic recombination (DR) reactions of $C_3H_2^+$ molecules. Same legend as Table 2. l refers to linear C_3H_2 isomers and c to the cyclic one.

Reaction	Model	KIDA	OSU	UDfA	$IP / \Delta E$
$c-C_3H_2^+ + e^- \rightarrow$					9.15
$c-C_3H/H$	0.34(\pm 0.08)	<u>0.36</u>	0.36	0.14	4.78
C_2H_2/C	0.27(\pm 0.03)	<u>0.07</u>	0.07	0.14	3.22
C_3/H_2	0.18(\pm 0.06)	<u>0.36</u>	0.36	0.28	5.97
$C_3/2H$	0.13(\pm 0.03)	<u>0.14</u>	0.14	0.28	1.35
C_2H/CH	0.05(\pm 0.01)				2.41
C_2/CH_2	0.03(\pm 0.01)	<u>0.07</u>	0.07	0.14	1.55
$l-C_3H_2^+ + e^- \rightarrow$					10.4
$C_3/2H$	0.39(\pm 0.04)	0.14	0.14	0.28	2.60
C_2H_2/C	0.38(\pm 0.06)	0.07	0.07	0.14	4.47
$l-C_3H/H$	0.07(\pm 0.06)	0.36	0.36	0.14	6.03
C_2H/CH	0.07(\pm 0.01)				3.66
C_2/CH_2	0.05(\pm 0.01)	0.07	0.07	0.14	2.80
C_3/H_2	0.04(\pm 0.01)	0.36	0.36	0.28	7.22

Table 5: Branching ratios for the charge exchange reactions between C_n and He^+ . Same legend as in Table 2 except for the last column. In column 6, $\Delta IP = IP(He) - IP(C_n)$ are reported in bold, together with in front of each channel exothermicities. All energies are in eV.

Reaction	Model	KIDA	OSU	UDfA	$\Delta IP / \Delta E$
$C_4 + He^+ \rightarrow$					13.1
C_3^+/C	0.61(\pm 0.06)	0.33	0.33	0.33	7.41
C_3/C^+	0.22(\pm 0.03)	0.33	0.33	0.33	7.87
C_2/C_2^+	0.16(\pm 0.03)	0.33	0.33	0.33	6.08
$C_2/C/C^+$	0.01(\pm 0.01)				0.62
$C_5 + He^+ \rightarrow$					13.6
C_3^+/C_2	0.47(\pm 0.10)	0.5	0.5	0.5	7.31
$C_3/C/C^+$	0.20(\pm 0.10)				1.77
C_4^+/C	0.14(\pm 0.04)	0.5	0.5	0.5	7.00
C_3/C_2^+	0.10(\pm 0.03)				7.24
$C_3^+/C/C$	0.09(\pm 0.06)				1.31
$C_6 + He^+ \rightarrow$					14.9
C_3^+/C_3	0.31(\pm 0.10)				8.68
$C_3^+/C_2/C$	0.19(\pm 0.06)				1.07
C_5^+/C	0.16(\pm 0.05)	0.5	0.5	0.5	7.84
$C_3/C_2/C^+$	0.16(\pm 0.04)				1.55
$C_3/C_2^+/C$	0.07(\pm 0.03)				1.18
C_4^+/C_2	0.07(\pm 0.04)	0.5	0.5	0.5	7.18
$C_4^+/C/C$	0.04(\pm 0.02)				1.09
$C_7 + He^+ \rightarrow$					14.5
C_4^+/C_3	0.40(\pm 0.08)				6.83
C_5^+/C_2	0.24(\pm 0.05)	0.5	0.5	0.5	5.98
$C_3^+/C_3/C$	0.14(\pm 0.05)				0.74
$C_3/C_3/C^+$	0.10(\pm 0.04)				1.21
C_4/C_3^+	0.08(\pm 0.02)				6.06
C_6^+/C	0.04(\pm 0.01)	0.5	0.5	0.5	6.96
$C_8 + He^+ \rightarrow$					15.4
$C_3^+/C_3/C_2$	0.47(\pm 0.07)				1.93
$C_4^+/C_3/C$	0.27(\pm 0.05)				1.95
C_5^+/C_3	0.13(\pm 0.09)				8.31
$C_5/C_2/C^+$	0.06(\pm 0.03)				1.17
$C_3/C_3/C_2^+$	0.04(\pm 0.01)				2.03
$C_4/C_3/C^+$	0.03(\pm 0.01)				1.65
C_6^+/C_2	0(\pm 0.005)	0.5	0.5	0.5	8.15
C_7^+/C	0(\pm 0.001)	0.5	0.5	0.5	9.62
$C_9 + He^+ \rightarrow$					15.2
$C_3^+/C_3/C_3$	0.49(\pm 0.03)				2.95
$C_5^+/C_3/C$	0.29(\pm 0.03)				2.12
$C_4^+/C_3/C_2$	0.20(\pm 0.03)				1.45
C_6^+/C_3	0.02(\pm 0.03)				8.98
C_8^+/C	0(\pm 0.001)	0.5	0.5	0.5	9.01
C_7^+/C_2	0(\pm 0.001)	0.5	0.5	0.5	8.92
$C_{10} + He^+ \rightarrow$					15.4
C_7^+/C_3	0.34(\pm 0.12)	0.55			8.35
$C_6^+/C_3/C$	0.23(\pm 0.07)	0.24			2.32
$C_4^+/C_3/C_3$	0.21(\pm 0.08)				0.70
C_5^+/C_5	0.13(\pm 0.05)	0.03			6.15
$C_7^+/C_2/C$	0.06(\pm 0.02)	19			1.50
C_6^+/C_4	0.02(\pm 0.02)	0.02			6.10
C_9^+/C	0.01(\pm 0.01)	0.03	0.5	0.5	6.90
C_8^+/C_2	0(\pm 0.005)	0.13	0.5	0.5	8.60

Table 6: Branching ratios for the charge exchange reactions between C_nH and He^+ . Same legend as Table 5.

Reaction	Model	KIDA	OSU	UDfA	$\Delta IP / \Delta E$
$C_2H + He^+ \rightarrow$					13.0
$C^+/C/H$	0.56(\pm 0.04)				1.84
CH^+/C	0.18(\pm 0.09)	0.33	0.33	0.33	6.11
C_2^+/H	0.16(\pm 0.08)	0.33	0.33	0.33	8.19
C_2/H^+	0.07(\pm 0.02)				6.00
C^+/CH	0.03(\pm 0.02)	0.33	0.33	0.33	5.49
$c-C_3H + He^+ \rightarrow$					15.5
$C_2^+/C/H$	0.45(\pm 0.05)				1.94
$C_2/C^+/H$	0.29(\pm 0.04)				2.09
C_3^+/H	0.06(\pm 0.04)	1.0	1.0		9.49
C_2H^+/C	0.06(\pm 0.04)				6.74
C_2^+/CH	0.05(\pm 0.03)				5.59
C_2H/C^+	0.03(\pm 0.02)				7.09
C_2/CH^+	0.03(\pm 0.02)				6.36
C_3/H^+	0.03(\pm 0.01)				7.50
$l-C_3H + He^+ \rightarrow$					16.2
$C_2^+/C/H$	0.54(\pm 0.03)				2.64
$C_2/C^+/H$	0.35(\pm 0.02)				2.79
$C/C/CH^+$	0.07(\pm 0.04)				0.55
C_3^+/H	0.02(\pm 0.02)	1.0	1.0		10.19
C_3/H^+	0.02(\pm 0.01)				8.20
$C_4H + He^+ \rightarrow$					12.6
$C_3^+/C/H$	0.46(\pm 0.05)				2.63
$C_3/C^+/H$	0.29(\pm 0.03)				2.98
$C_2^+/C_2/H$	0.16(\pm 0.04)				1.58
C_3H^+/C	0.04(\pm 0.04)				9.14
C_2H^+/C_2	0.04(\pm 0.02)	0.5	0.5	0.5	6.39
C_4^+/H	0.01(\pm 0.02)	0.5	0.5	0.5	8.78

Table 7: Branching ratios for the charge exchange reactions between C_3H_2 and He^+ . Same legend as Table 5.

Reaction	Model	KIDA	OSU	UDfA	$\Delta IP / \Delta E$
$l-C_3H_2 + He^+ \rightarrow$					14.15
$C_2H^+/C/H$	0.25(\pm 0.05)				1.45
$C_3^+/H/H$	0.24(\pm 0.03)				4.05
$C_2H/C^+/H$	0.15(\pm 0.03)				1.35
$C_3/H^+/H$	0.10(\pm 0.02)				2.05
$C_2/C^+/H_2$	0.10(\pm 0.02)				1.95
C_2H^+/CH	0.06(\pm 0.02)				4.95
$C_2/CH^+/H$	0.06(\pm 0.03)				0.75
$C_2H_2^+/C$	0.04(\pm 0.01)				5.95
C_3H^+/H	0.(\pm 0.004)	0.5	0.5	1.0	9.85
C_3^+/H_2	0.(\pm 0.002)	0.5	0.5		8.55
$c-C_3H_2 + He^+ \rightarrow$					15.43
$C_2H^+/C/H$	0.28(\pm 0.03)				2.73
$C_2/CH^+/H$	0.16(\pm 0.02)				2.03
$C_3^+/H/H$	0.14(\pm 0.02)				5.33
$C_2^+/CH/H$	0.14(\pm 0.02)				1.23
$C_2H/C^+/H$	0.13(\pm 0.02)				3.13
$C_2/C^+/H_2$	0.08(\pm 0.01)				3.23
$C_3/H^+/H$	0.07(\pm 0.01)				3.33
C_3H^+/H	0.(\pm 0.001)	0.5	0.5	1.0	11.13
C_3^+/H_2	0.(\pm 0.001)	0.5	0.5		9.83

Table 8: Branching ratios for the reactions between C^+ and C_n . Same legend as Table 2. Pathways indicated by †, §, or \diamond are forbidden in ground states (see appendix A). In column 6, the association energies E_{as} (see text), are reported in bold, together with in front of each channel exothermicities. All energies are in eV.

Reaction	Model	KIDA	OSU	UDfA	$E_{as} / \Delta E$
$C_3 + C^+ \rightarrow$					5.62
C_3/C^+	1.0(\pm 0.01)				0
$C_4 + C^+ \rightarrow$					7.04
C_3^+/C_2	0.79(\pm 0.07)				0.27
† C_3/C_2^+	0.11(\pm 0.05)				0.38
C_4^+/C	0.10(\pm 0.05)				0.29
C_5^+	0	1.0	1.0	1.0	
$C_5 + C^+ \rightarrow$					6.97
C_3^+/C_3	1.0(\pm 0.01)				0.74
C_6^+	0	1.0	1.0	1.0	
$C_6 + C^+ \rightarrow$					8.94
C_4^+/C_3	0.78(\pm 0.04)				1.27
C_5^+/C_2	0.11(\pm 0.04)				0.42
C_4/C_3^+	0.06(\pm 0.02)				0.50
C_6^+/C	0.05(\pm 0.01)				1.40
C_7^+	0	1.0	1.0	1.0	
$C_7 + C^+ \rightarrow$					8.05
C_5^+/C_3	0.90(\pm 0.02)				1.16
C_5/C_3^+	0.05(\pm 0.01)				0.77
C_6^+/C_2	0.05(\pm 0.01)				0.62
C_8^+	0	1.0	1.0	1.0	
$C_8 + C^+ \rightarrow$					8.60
C_6^+/C_3	0.66(\pm 0.03)				2.5
C_7^+/C_2	0.15(\pm 0.01)				2.3
C_5^+/C_4	0.11(\pm 0.02)				1.0
C_8^+/C	0.04(\pm 0.01)				2.3
C_5/C_4^+	0.04(\pm 0.01)				0.9
C_9^+	0	1.0	1.0	1.0	
$C_9 + C^+ \rightarrow$					10.4
C_{10}^+	0	1.0	1.0	1.0	
C_7^+/C_3	0.79(\pm 0.03)				3.3
C_5^+/C_5	0.12(\pm 0.02)				1.15
C_6^+/C_4	0.05(\pm 0.02)				1.1
C_9^+/C	0.04(\pm 0.02)				1.9

Table 9: Branching ratios for the reactions between C^+ and C_nH . Same legend as Table 8.

Reaction	Model	KIDA	OSU	UDfA	$E_{ass} / \Delta E$
$CH + C^+ \rightarrow$					7.51
CH^+/C	0.53(\pm 0.03)	0.5	0.5	0.5	0.61
C_2^+/H	0.43(\pm 0.05)	0.5	0.5	0.5	2.70
C_2/H^+	0.04(\pm 0.03)				0.51
$C_2H + C^+ \rightarrow$					8.41
C_3^+/H	0.96(\pm 0.02)	1.0	1.0	1.0	2.40
C_3/H^+	0.04(\pm 0.02)				0.41
l&c-$C_3H + C^+ \rightarrow$					6.16
C_3H^+/C	0.50(\pm 0.03)				2.7
C_4^+/H	0.35(\pm 0.03)	1.0	1.0		2.34
C_3/CH^+	0.15(\pm 0.03)				0.81
$C_2H_2 + C^+ \rightarrow$					6.7
C_3H^+/H	1.0(\pm 0.01)	<u>1.0</u>	1.0	1.0	2.1

 Table 10: Branching ratios for the reactions between H^+ and C_n and C_nH . Same legend as Table 8.

Reaction	Model	KIDA	OSU	UDfA	$E_{ass} / \Delta E$
$C_2 + H^+ \rightarrow$					7.00
${}^\dagger C_2^+/H$	0.80(\pm 0.09)	1.0	1.0	1.0	2.19
${}^\dagger CH^+/C$	0.20(\pm 0.09)				0.11
$C_3 + H^+ \rightarrow$					8.00
${}^\S C_3^+/H$	1.00(\pm 0.01)	1.0	1.0	1.0	1.99
$C_4 + H^+ \rightarrow$					6.47
${}^\dagger C_3H^+/C$	0.44(\pm 0.04)				3.01
C_4^+/H	0.31(\pm 0.03)	1.0	1.0	1.0	2.65
C_3/CH^+	0.15(\pm 0.02)				0.15
l&c - C_3H/C^+	0.05(\pm 0.05)				0.31
l&c-$C_3H + H^+ \rightarrow$					8.70
${}^\S C_3H^+/H$	0.59(\pm 0.04)	0.5	0.5		4.40
C_3^+/H_2	0.28(\pm 0.03)	0.5	0.5		2.50*
C_2H_2/C^+	0.05(\pm 0.01)				2.40
$C_2H_2^+/C$	0.04(\pm 0.04)				1.70
${}^\S \diamond C_2H/CH^+$	0.04(\pm 0.04)				0.47

Table 11: Branching ratios for the reactions between C_2^+ and C_nH_m . Same legend as Table 8.

Reaction	Model	KIDA	OSU	UDfA	$E_{ass} / \Delta E$
C + C₂⁺ →					7.49
§C ₂ /C ⁺	1.0	1.0	1.0	1.0	0.37
C₂ + C₂⁺ →					7.51
C ₃ ⁺ /C	0.74(± 0.05)	1.0	1.0	1.0	1.41
†C ₃ /C ⁺	0.26(± 0.05)				1.89
CH + C₂⁺ →					9.91
C ₂ H ⁺ /C	0.33(± 0.03)				1.15
C ₃ ⁺ /H	0.30(± 0.02)	0.5	0.5	0.5	3.90
C ₂ H/C ⁺	0.19(± 0.02)				1.50
†C ₂ /CH ⁺	0.15(± 0.03)	0.5	0.5	0.5	0.77
†C ₃ /H ⁺	0.03(± 0.01)				1.91
CH₂ + C₂⁺ →					8.38
C ₃ H ⁺ /H	0.65(± 0.04)	0.5	0.5		4.40
C ₃ ⁺ /H ₂	0.30(± 0.04)				2.50
C ₂ H ₂ /C ⁺	0.05(± 0.01)				2.40
CH ₂ ⁺ /C ₂	0.0(± 0.001)	0.5	0.5		0.3

Table 12: Branching ratios for the reactions between CH⁺ and C_nH_m . Same legend as Table 8.

Reaction	Model	KIDA	OSU	UDfA	$E_{ass} / \Delta E$
C + CH⁺ →					6.89
C ₂ ⁺ /H	0.95(± 0.02)	1.0	1.0	1.0	2.08
†C ₂ /H ⁺	0.05(± 0.02)				0.37
C₂ + CH⁺ →					9.14
§C ₃ ⁺ /H	0.50(± 0.05)	1.0	1.0	1.0	3.13
C ₂ H/C ⁺	0.27(± 0.05)				0.73
C ₂ H ⁺ /C	0.18(± 0.07)				0.38
C ₃ /H ⁺	0.05(± 0.02)				1.14
C₂H + CH⁺ →					8.2
C ₃ H ⁺ /H	0.65(± 0.04)				3.8
§C ₃ ⁺ /H ₂	0.30(± 0.04)	1.0	1.0	1.0	1.4
C ₂ H ₂ /C ⁺	0.05(± 0.01)				1.5

Table 13: Branching ratios for the reactions between C_2H^+ , $C_2H_2^+$ and C or CH. Same legend as Table 8.

Reaction	Model	OSU	UDfA	$E_{ass} / \Delta E$
C + C₂H⁺ →				8.76
C ₃ ⁺ /H	0.78(± 0.07)	1.0	1.0	0.37
C ₂ H/C ⁺	0.16(± 0.06)			0.37
C ₃ /H ⁺	0.06(± 0.02)			2.08
CH + C₂H⁺ →				9.2
C ₃ H ⁺ /H	0.55(± 0.04)	0.5	0.5	4.9
C ₃ ⁺ /H ₂	0.27(± 0.03)			2.4
C ₂ H ₂ ⁺ /C	0.07(± 0.01)			0.82
C ₂ H ₂ /C ⁺	0.07(± 0.01)			1.0
C ₂ H/CH ⁺	0.04(± 0.01)			1.0
C ₂ /CH ₂ ⁺		0.5	0.5	1.0
C + C₂H₂⁺ →				8.2
C ₃ H ⁺ /H	0.65(± 0.04)	0.33	1.0	3.8
C ₃ ⁺ /H ₂	0.30(± 0.04)	0.33		1.4
C ₂ H ₂ /C ⁺	0.05(± 0.01)	0.33		1.5

 Table 14: Branching ratios (BR) for the neutral-neutral reactions between C_nH_m and C. Same legend as Table 2. Pathways indicated by †, §, or ◇ are forbidden in ground states (see appendix A). In column 6, the association energies (E_{ass}) are reported in bold, together with in front of each channel exothermicities. All energies are in eV.

Reaction	Model	KIDA	OSU	UDfA	$E_{ass} / \Delta E$
C + C₄ →					6.97
†C ₃ /C ₂	1.0	1.0	1.0	1.0	1.2
C + C₅ →					5.46
†C ₃ /C ₃	1.0	1.0	1.0	1.0	2.5
C + C₆ →					6.33
†C ₄ /C ₃	0.87(± 0.04)	0.5	0.5		0.5
†C ₅ /C ₂	0.13(± 0.04)	0.5	0.5		0.8
C + C₇ →					5.48
†C ₃ /C ₅	1.0	1.0	1.0		1.5
C + C₈ →					6.7
†C ₆ /C ₃	0.67(± 0.04)	0.3	0.3		1.1
†C ₅ /C ₄	0.31(± 0.04)	0.3	0.3		0.8
†C ₇ /C ₂	0.02(± 0.01)	0.3	0.3	1.0	0.3
C + C₉ →					6.0
†C ₅ /C ₅	0.87(± 0.04)				1.2
†C ₃ /C ₇	0.13(± 0.04)				1.2
C + CH →					7.86
C ₂ /H	1.0	1.0	1.0	1.0	2.8
C + C₂H →					6.21
§C ₃ /H	1.0	1.0	1.0	1.0	2.75
C + l&c-C₃H →					6.90
C ₄ /H	0.91(± 0.04)	1.0	1.0		2.0
C ₂ H/C ₂	0.09(± 0.04)				0.3
C + C₂H₂ →					5.93
†C ₃ /H ₂	0.35(± 0.04)	<u>0.73</u>	0.73	0.5	1.5
(1 + c)C ₃ H/H	0.65(± 0.04)	<u>0.27</u>	0.27	0.5	1.5

Table 15: Branching ratios for the neutral-neutral reactions between C_nH_m and CH or C_2H . Same legend as Table 14.

Reaction	model	OSU	UMI	$\overline{E_{ass}/\Delta E}$
$C_2 + CH \rightarrow$				7.57
C_3/H	0.63(\pm 0.04)	1.0	1.0	4.1
C_2H/C	0.37(\pm 0.04)			1.4
$C_3 + CH \rightarrow$				6.71
${}^sC_4/H$	0.99(\pm 0.01)	1.0	1.0	1.84
C_2H/C_2	0.01(\pm 0.01)			0.1
$C_2 + C_2H \rightarrow$				6.61
C_4/H	1.0	1.0	1.0	1.74

Table 16: Branching ratios (BR) for the ion pair reactions between C_n^- and C^+ . Same legend as Table 8.

Reaction	model	KIDA & OSU	$E_{ass}/\Delta E$
$C_3^- + C^+ \rightarrow$			14.33
${}^{\S}C_2/C/C$	0.80(\pm 0.10)		2.25
${}^{\S}C_3/C$	0.15(\pm 0.10)	1.0	9.51
${}^{\S}C_2/C_2$	0.05(\pm 0.04)		8.24
$C_4^- + C^+ \rightarrow$			14.78
${}^{\S}C_3/C/C$	0.60(\pm 0.07)		2.98
${}^{\S}C_2/C_2/C$	0.34(\pm 0.04)		1.72
${}^{\S}C_3/C_2$	0.06(\pm 0.07)		9.27
${}^{\S}C_4/C$	0.0(\pm 0.004)	1.0	7.81
$C_5^- + C^+ \rightarrow$			14.18
$C_3/C_2/C$	0.79(\pm 0.05)		2.91
$C_2/C_2/C_2$	0.10(\pm 0.03)		1.65
$C_4/C/C$	0.08(\pm 0.03)		1.75
C_3/C_3	0.03(\pm 0.05)		10.18
C_5/C	0.0(\pm 0.007)	1.0	8.72
$C_6^- + C^+ \rightarrow$			13.87
$C_3/C_3/C$	0.53(\pm 0.03)		3.54
$C_3/C_2/C_2$	0.40(\pm 0.03)		2.26
$C_4/C_2/C$	0.05(\pm 0.02)		1.10
C_5/C_2	0.02(\pm 0.02)		8.07
C_6/C	0.00(\pm 0.001)	1.0	7.54
$C_7^- + C^+ \rightarrow$			13.99
$C_3/C_3/C_2$	0.72(\pm 0.03)		3.11
$C_4/C_3/C$	0.21(\pm 0.03)		2.36
$C_5/C_2/C$	0.05(\pm 0.02)		1.88
C_5/C_3	0.02(\pm 0.003)		9.49
C_7/C	0.0(\pm 0.003)	1.0	8.24
$C_8^- + C^+ \rightarrow$			14.06
${}^{\S}C_3/C_3/C_3$	0.52(\pm 0.06)		2.09
${}^{\S}C_4/C_3/C_2$	0.17(\pm 0.04)		1.81
${}^{\S}C_6/C_3$	0.15(\pm 0.09)		8.44
${}^{\S}C_5/C_3/C$	0.14(\pm 0.02)		2.86
${}^{\S}C_7/C_2$	0.02(\pm 0.01)		7.69
${}^{\S}C_8/C$	0.0(\pm 0.002)	1.0	7.36
$C_9^- + C^+ \rightarrow$			14.18
$C_4/C_3/C_3$	0.35(\pm 0.23)		7.36
C_7/C_3	0.30(\pm 0.39)		7.36
$C_5/C_3/C_2$	0.20(\pm 0.13)		7.36
C_5/C_5	0.11(\pm 0.04)		7.36
$C_6/C_3/C$	0.02(\pm 0.02)		7.36
$C_5/C_4/C$	0.02(\pm 0.02)		7.36
C_9/C	0.0(\pm 0.001)	1.0	7.36

Table 17: Measured branching ratios (BR,%) for de-excitation channels of C_4^+ following excitation in C_4^+ –He collision ($v = 2.6$ velocity atomic units (*au*)). Absolute 1σ errors are given in parenthesis. The dissociation energies are reported in columns 3 and 6 in eV from Díaz-Tendero et al. (2006b).

Channel	BR	E_{diss}	Channel	BR	E_{diss}
C_3^+/C	19.6 (0.8)	5.7	C_3/C^+	7.2 (0.7)	5.2
C_2^+/C_2	5.2 (1.2)	7.0	$C_2/C^+/C$	35.0 (0.7)	12.5
$C_2^+/2C$	13.1 (0.4)	13.0	$C^+/3C$	18.5 (0.8)	12.8

Table 18: Measured branching ratios (BR,%) for de-excitation channels of C_5^+ following excitation in C_5^+ –He collision ($v = 2.6$ *au*). Same legend as Table 17.

Channel	BR	E_{diss}	Channel	BR	E_{diss}
C_3^+/C_2	17.8 (1.1)	6.8	C_3/C_2^+	4.9 (0.4)	6.7
C_4^+/C	6.75 (0.4)	6.7	C_4/C^+	1.4 (0.2)	7.0
$C_3^+/C^+/C$	13.9 (0.8)	12.4	$C_3^+/2C$	13.2 (0.8)	12.8
$2C_2^+/C^+$	5.9 (0.4)	13.9	$C_2^+/C_2^+/C$	11.3 (0.5)	14.3
$C_2^+/C^+/2C$	14.9 (0.9)	20.0	$C_2^+/3C$	5.4 (0.4)	20.3
$C^+/4C$	4.9 (0.4)	26.0			

Table 19: Measured branching ratios (BR,%) for de-excitation channels of C_6^+ following excitation in C_6^+ –He collision ($v = 2.6$ *au*). Same legend as Table 17.

Channel	BR	E_{diss}	Channel	BR	E_{diss}
C_3^+/C_3	22.8(2.0)	6.2	C_5^+/C	6.5(0.5)	7.1
C_5^+/C^+	0.4(0.1)	7.0	C_4^+/C_2	4.5(0.5)	7.7
C_4^+/C_2^+	0.7(0.1)	8.4	$C_3^+/C_2^+/C^+$	9.1(0.7)	13.4
$C_3^+/C_2^+/C$	17.3(1.5)	13.8	$C_3^+/C_2^+/C$	5.3(0.5)	13.7
$C_4^+/2C$	4.1(0.4)	13.8	$C_4^+/C^+/C$	1.3(0.2)	14.1
$C_2^+/2C_2$	1.9(0.2)	15.2	$C_3^+/C^+/2C$	6.8(0.5)	19.4
$C_3^+/3C$	3.9(0.4)	19.9	$2C_2^+/C^+/C$	4.9(0.4)	21.0
$C_2^+/C_2^+/2C$	4.4(0.4)	21.3	$C_2^+/C^+/3C$	4.1(0.4)	27.0
$C_2^+/4C$	1.3(0.2)	27.4	$C^+/5C$	1.1(0.2)	33.1

Table 20: Measured branching ratios (BR,%) for de-excitation channels of C_7^+ following excitation in C_7^+ –He collision ($v = 2.6 au$). Same legend as Table 17.

Channel	BR	E_{diss}	Channel	BR	E_{diss}
C_6^+/C	1.8(0.2)	7.5	C_4^+/C_3	18.5 (0)	7.7
C_4/C_3^+	2.5(0.3)	8.4	C_5^+/C_2	6.7(0.5)	8.5
C_5/C_2^+	0.2(0.1)	8.8	C_6^+/C	0.1(0.1)	8.9
$2C_3/C^+$	5.1(0.4)	13.3	$C_3^+/C_3/C$	15.5(1.0)	13.8
$C_5/C^+/C$	0.4(0.1)	14.5	$C_5^+/2C$	3.0(0.3)	14.6
$C_3/C_2^+/C_2$	2.9(0.3)	15.2	$C_4^+/C_2/C$	4.5(0.4)	15.3
$C_3^+/2C_2$	6.7(0.5)	15.3	$C_4/C_2/C^+$	1.0(0.1)	15.6
$C_4/C_2^+/C$	0.5(0.1)	15.9	$C_3/C_2/C^+/C$	7.6(0.5)	20.9
$C_3/C_2^+/2C$	2.5(0.2)	21.3	$C_4^+/3C$	1.1(0.1)	21.4
$C_3^+/C_2/2C$	7.1(0.3)	21.4	$C_4/C^+/2C$	0.3(0.1)	21.6
$3C_2/C^+$	0.8(0.1)	22.4	$C_2^+/2C_2/C$	1.9(0.2)	22.8
$C_3/C^+/3C$	2.1(0.2)	27.0	$C_3^+/4C$	1.2(0.1)	27.5
$2C_2/C^+/2C$	2.7(0.3)	28.5	$C_2^+/C_2/3C$	1.6(0.2)	28.8
$C_2/C^+/4C$	1.6(0.2)	34.6	$C_2^+/5C$	0.3(0.1)	34.9
$C^+/6C$	0.3(0.1)	40.7			

Table 21: Measured branching ratios (BR,%) for de-excitation channels of C_8^+ following excitation in C_8^+ –He collision ($v = 2.6 au$). Same legend as Table 17.

Channel	BR	E_{diss}	Channel	BR	E_{diss}
C_7^+/C	2.3(0.3)	5.8	C_5^+/C_3	26.0(1.6)	6.7
C_5/C_3^+	1.5(0.1)	7.1	C_6^+/C_2	1.9(0.2)	7.25
C_4^+/C_4	1.4(0.1)	8.1	$C_6^+/2C$	0.7(0.1)	13.3
$2C_3/C_2^+$	1.6(0.2)	13.4	$C_4^+/C_3/C$	8.7(0.6)	13.4
$C_3^+/C_3/C_2$	16.2(1.0)	13.5	$C_4/C_3/C^+$	1.3(0.1)	13.8
$C_4/C_3^+/C$	1.6(0.2)	14.2	$C_5/C_2/C^+$	0.3(0.1)	14.2
$C_5^+/C_2/C$	4.4(0.3)	14.3	$C_5/C_2^+/C$	0.2(0.1)	14.6
$C_4^+/2C_2$	1.1(0.1)	15.0	$C_4/C_2^+/C_2$	0.3(0.1)	15.6
$2C_3/C^+/C$	3.3(0.3)	19.1	$C_3^+/C_3/2C$	5.3(0.4)	19.5
$C_5/C^+/2C$	0.1(0.1)	20.3	$C_5^+/3C$	0.7(0.1)	20.4
$C_3/2C_2/C^+$	1.9(0.2)	20.6	$C_3C_2^+/C_2C$	2.1(0.2)	21.0
$C_4^+/C_2/2C$	1.7(0.2)	21.0	$C_3^+/2C_2/C$	4.2(0.3)	21.1
$C_4C_2/C^+/C$	0.5(0.1)	21.4	$C_4/C_2^+/2C$	0.2(0.1)	21.7
C_3C_2/C^+2C	2.9(0.2)	26.7	$C_3/C_2^+/3C$	0.7(0.1)	27.0
$C_4^+/4C$	0.2(0.1)	27.1	$C_3^+/C_2/3C$	2.0(0.2)	27.2
$3C_2/C^+/C$	0.7(0.1)	28.2	$C_2^+/2C_2/2C$	0.8(0.1)	28.6
$C_3/C^+/4C$	0.6(0.1)	32.8	$C_3^+/5C$	0.2(0.1)	33.2
$2C_2/C^+/3C$	0.9(0.1)	34.3	$C_2^+/C_2/4C$	0.5(0.1)	34.7
$C_2/C^+/5C$	0.5(0.1)	40.4	$C^+/7C$	0.1(0.1)	46.4

Table 22: Measured branching ratios (BR,%) for de-excitation channels of C_9^+ following excitation in C_9^+ –He collision ($v = 2.6$ au). Same legend as Table 17.

Channel	BR	E_{diss}	Channel	BR	E_{diss}
C_8^+/C	0.9(0.1)	6.2	C_7^+/C_2	3.4(0.8)	6.3
C_6^+/C_3	17.5(2.8)	6.2	C_5^+/C_4	2.7(0.3)	7.8
C_5^+/C_4^+	1.0(0.1)	7.7	$C_7^+/2C$	0.8(0.1)	12.2
$C_6^+/C_2/C$	1.3(0.2)	13.7	$C_5^+/C_3/C$	9.2(0.8)	13.1
$C_5^+/C_3^+/C$	0.7(0.1)	13.5	$C_5^+/C_3/C^+$	0.5(0.1)	13.2
$C_5^+/2C_2$	1.7(0.2)	14.8	$C_4^+/C_4/C$	0.5(0.1)	14.5
$C_4^+/C_3/C_2$	7.0(0.6)	14.0	$C_4^+/C_3^+/C_2$	1.6(0.2)	14.7
$C_4^+/C_3/C_2^+$	0.4(0.1)	14.5	$C_3^+/2C_3$	16.4(1.3)	12.5
$C_6^+/3C$	0.3(0.1)	19.7	$C_5^+/C_2/2C$	1.3(0.1)	20.7
$C_5C_2C^+/C$	0.2(0.1)	20.6	$C_4^+/C_3/2C$	2.3(0.2)	19.8
$C_4^+/C_3^+/2C$	0.6(0.1)	20.6	$C_4C_3C^+/C$	0.7(0.1)	20.1
$C_4^+/2C_2/C$	0.9(0.1)	21.3	$C_4C_2^+C_2/C$	0.3(0.1)	22.3
$C_4^+/2C_2/C^+$	0.2(0.1)	21.8	$C_3^+C_3C_2/C$	9.2(0.7)	19.8
$2C_3^+/C_2^+/C$	1.0(0.2)	19.8	$2C_3^+/C_2/C^+$	2.7(0.3)	19.4
$C_3^+/3C_2$	0.8(0.1)	21.4	$C_3^+/C_2^+/2C_2$	0.5(0.1)	21.3
$C_5^+/4C$	0.2(0.1)	26.8	$C_4^+/C_2/3C$	0.5(0.1)	27.4
$C_4^+/C_2^+/3C$	0.1(0.1)	28.1	$C_4C_2C^+/2C$	0.3(0.1)	27.7
$C_3^+/C_3^+/3C$	1.8(0.2)	25.9	$2C_3^+/C^+/2C$	1.5(0.2)	28.5
$C_3^+/2C_2/2C$	2.0(0.2)	27.5	$C_3C_2^+C_2/2C$	1.1(0.1)	27.3
$C_3^+2C_2C^+/C$	1.5(0.2)	27.0	$C_2^+/3C_2/C$	0.2(0.1)	28.9
$C_4^+/C^+/4C$	0.1(0.1)	33.8	$C_3^+/C_2/4C$	0.6(0.1)	32.8
$C_3^+/C_2^+/4C$	0.2(0.1)	33.4	$C_3C_2C^+/3C$	1.2(0.1)	33.1
$C_2^+/2C_2/3C$	0.3(0.1)	34.9	$3C_2^+/C^+/2C$	0.4(0.1)	34.6
$C_3^+/6C$	0.1(0.1)	39.6	$C_3^+/C^+/5C$	0.1(0.1)	39.1
$C_2^+/C_2/5C$	0.2(0.1)	41.0	$2C_2^+/C^+/4C$	0.5(0.1)	40.7
$C_2^+/C^+/6C$	0.1(0.1)	46.7	$C^+/8C$	0(0.1)	52.8

Table 23: Measured branching ratios (BR,%) for de-excitation channels of C_{10}^+ following excitation in C_{10}^+ -He collision ($v = 2.6 au$). Same legend as Table 17.

Channel	BR	E_{diss}	Channel	BR	E_{diss}
C_9^+/C	0.7(0.2)	8.5	C_8^+/C_2	0.6(0.2)	6.8
C_7^+/C_3	19.5(5.3)	7.1	C_7^+/C_3^+	0.1(0.1)	9.6
C_6^+/C_4	1.0(0.2)	9.3	C_5^+/C_5	3.0(0.4)	9.2
$C_7^+/C_2/C$	1.4(0.3)	14.8	$C_6^+/C_3/C$	5.0(0.6)	14.6
$C_6^+/2C_2$	0.3(0.1)	14.2	$C_5^+/C_4/C$	0.8(0.2)	16.3
$C_5^+/C_4^+/C$	0.4(0.1)	16.2	$C_5^+/C_4/C^+$	0.1(0.1)	16.3
$C_5^+/C_3/C_2$	10.3(1.1)	13.7	$C_5^+/C_3^+/C_2$	1.0(0.2)	16.0
$C_5^+/C_3/C_2^+$	0.2(0.1)	15.9	$C_4^+/C_4/C_2$	0.4(0.1)	15.1
$C_4^+/2C_3$	13.6(1.4)	14.7	$C_4^+/C_3^+/C_3$	4.1(0.4)	15.5
$C_7^+/3C$	0.3(0.2)	20.67	$C_6^+/C_2/2C$	0.3(0.1)	21.44
$C_5^+/C_3/2C$	2.2(0.3)	21.6	$C_5^+/C_3^+/2C$	0.1(0.1)	22.5
$C_5C_3C^+/C$	0.2(0.1)	21.6	$C_5^+/2C_2/C$	0.8(0.2)	21.3
$C_4^+/C_4/2C$	0.1(0.1)	23.0	$2C_4/C^+/C$	0.1(0.1)	23.3
$C_4^+C_3C_2/C$	3.5(0.4)	20.4	$C_4C_3^+C_2/C$	0.6(0.2)	23.2
$C_4C_3C_2^+/C$	0.3(0.1)	23.0	$C_4C_3C_2/C^+$	0.5(0.1)	20.7
$C_4^+/3C_2$	0.2(0.1)	21.9	$C_3^+/2C_3/C$	6.2(0.6)	20.8
$3C_3/C^+$	1.2(0.2)	20.3	$C_3^+/C_3/2C_2$	4.3(0.5)	20.4
$2C_3/C_2^+/C_2$	0.8(0.2)	20.4	$C_5^+/C_2/3C$	0.4(0.1)	29.2
$C_5C_2C^+/2C$	0.1(0.1)	28.4	$C_4^+/C_3/3C$	0.7(0.2)	28.3
$C_4/C_3^+/3C$	0.1(0.1)	29.1	$C_4C_3C^+/2C$	0.2(0.1)	28.6
$C_4^+/2C_2/2C$	0.5(0.2)	29.2	$C_4C_2^+C_2/2C$	0.1(0.1)	29.8
$C_42C_2C^+/C$	0.1(0.1)	28.3	$C_3^+C_3C_2/2C$	3.4(0.4)	27.7
$2C_3/C_2^+/2C$	0.4(0.1)	28.2	$2C_3C_2C^+/C$	2.1(0)	26.1
$C_3^+3C_2/C$	0.7(0.1)	28.0	$C_3C_2^+2C_2/C$	0.6(0.2)	27.9
$C_3/3C_2/C^+$	0.4(0.1)	27.5	$C_2^+/4C_2$	0.1(0.1)	29.4
$C_5^+/5C$	0.1(0.1)	35.3	$C_4^+/C_2/4C$	0.2(0.1)	35.9
$C_4C_2C^+/3C$	0.1(0.1)	36.2	$C_3^+/C_3/4C$	0.5(0.1)	34.4
$2C_3/C^+/3C$	0.6(0.1)	34.0	$C_3^+/2C_2/3C$	0.7(0.1)	35.9
$C_3C_2^+C_2/3C$	0.5(0.1)	35.8	$C_32C_2C^+2C$	0.7(0.1)	34.8
$C_2^+/3C_2/2C$	0.1(0.1)	36.7	$4C_2/C^+/C$	0.1(0.1)	35.2
$C_3^+/C_2/5C$	0.3(0.1)	42.0	$C_3C_2C^+4C$	0.5(0.1)	41.6
$C_2^+/2C_2/4C$	0.2(0.1)	43.5	$3C_2/C^+/3C$	0.3(0.1)	43.0
$C_2^+/C_2/6C$	0.1(0.1)	49.5	$2C_2/C^+/5C$	0.1(0.1)	49.2
$C_2/C^+/7C$	0.1(0.1)	55.2	$C^+/9C$	0	61.3

Table 24: Measured branching ratios (BR,%) for de-excitation channels of C_3H_2 following charge transfer in $C_3H_2^+ - He$ collision ($v = 2.6 au$). Absolute 1σ errors are given in parenthesis. The energies of dissociation are reported in columns 3 and 6 in eV from Mebel et al. (1998).

Channel	BR	E_{diss}	Channel	BR	E_{diss}
C_3H_2	18.8(6.5)		C_3H/H	19.3(5.4)	4.4
C_3/H_2	9.9(3.9)	4.4	C_2H_2/C	9.8(4.0)	5.9
C_2H/CH	1.6(1.6)	6.7	C_2/CH_2	1.4(1.4)	7.6
$C_3/2H$	15.8(6.2)	7.8	$C_2H/C/H$	8.2(4.3)	10.2
$C_2/CH/H$	2.1(2.1)	11.9	$C_2/C/H_2$	0.9(0.9)	10.1
$2CH/C$	0.1(0.2)	13.5	$CH_2/2C$	0.1(0.2)	14.5
$C_2/C/2H$	5.2(1.1)	14.9	$2C/CH/H$	2.8(0.7)	17.8
$3C/2H$	4.0(0.4)	21.4			

Table 25: Measured branching ratios (BR,%) for de-excitation channels of $C_3H_2^+$ following excitation in $C_3H_2^+ - He$ collision ($v = 2.6 au$). Absolute 1σ errors are given in parenthesis. In columns 3 and 6 are reported the energies of dissociation (eV) using neutral dissociation energies from Mebel et al. (1998) and ionization potentials from Clauberg et al. (1992).

Channel	BR	E_{diss}	Channel	BR	E_{diss}
H/C_3H^+	19.2(1.0)	4.3	H_2/C_3^+	5.1(0.5)	5.6
CH/C_2H^+	3.3(0.5)	9.2	$C/C_2H_2^+$	2.3(0.5)	8.2
C_2H/CH^+	1.9(0.4)	8.2	C_2H_2/C^+	1.6(0.3)	8.0
CH_2/C_2^+	0.4(0.2)	9.9	C_2/CH_2^+	0.4(0.1)	8.8
C_3H/H^+	0.1(0.2)	8.7	$2H/C_3^+$	6.8(0.5)	10.1
$C/H/C_2H^+$	6.3(0.6)	12.7	$C/CH/CH^+$	5.2(1.0)	16.1
$CH/H/C_2^+$	4.1(0.4)	14.2	$C_2/H/CH^+$	3.4(0.4)	13.4
$C_2H/H/C^+$	3.2(0.7)	12.3	$C_2H/C/H^+$	3.2(0.4)	14.6
$C_3/H/H^+$	2.6(0.3)	12.1	$2CH/C^+$	2.6(0.5)	16.7
$C_2/H_2/C^+$	2.5(0.2)	12.2	$C/CH_2/C^+$	1.3(0.4)	15.6
$C/H_2/C_2^+$	0.8(0.1)	12.5	$C_2/CH/H^+$	0.6(0.2)	16.4
$2C/CH_2^+$	0.3(0.3)	14.6	$C/2H/C_2^+$	6.1(0.3)	16.8
$C_2/2H/C^+$	4.1(0.1)	16.7	$C_2/C/H/H^+$	2.5(0.4)	19.0
$CH/C/H/C^+$	2.2(0.7)	19.8	$2C/H/CH^+$	2.1(0.5)	19.2
$2C/H_2/C^+$	1.4(0.3)	17.9	$2C/CH/H^+$	0.3(0.4)	22.2
$2C/2H/C^+$	2.6(0.3)	24.3	$3C/H/H^+$	1.7(0.2)	26.7